



OPEN Design, synthesis, and evaluation of triazolo[1,5-*a*]pyridines as novel and potent α -glucosidase inhibitors

Fariba Peytam^{1,2}, Parham Foroumadi³, Hayrettin Ozan Gulcan^{4,5}, Maryam Norouzbahari⁶, Somayeh Mojtabavi⁷, Mohammad Ali Faramarzi⁷, Fahimeh Ghasemi⁸, Mohammadreza Torabi⁸, Behnaz Bameri⁹, Maliheh Barazandeh Tehrani¹, Loghman Firoozpour^{1,2}✉ & Alireza Foroumadi^{1,2}✉

α -Glucosidase is a key enzyme responsible for controlling the blood glucose, making a pivotal target in the treatment of type 2 diabetes mellitus. Present work introduces^{1,2,4} triazolo[1,5-*a*]pyridine as a novel, potent scaffold for α -glucosidase inhibition. A diverse scope of targeted compounds was prepared through an efficient, straightforward synthetic protocol. A series of compounds (15a–15v) were synthesized using a simple and efficient protocol, all showing notable inhibitory activity. Among them, compound 15j exhibited the best inhibition potency ($IC_{50} = 6.60 \pm 0.09 \mu M$), acting as a competitive and selective α -glucosidase inhibitor with no effect on α -amylase. Moreover, comprehensive computational studies were performed to validate the in vitro results and provide insight into compounds' binding interactions within the α -glucosidase's active site. The machine learning model, trained with the Estate fingerprint, achieved an AUC score of 0.65, demonstrating its utility in predicting α -glucosidase inhibition. Random Forest was identified as the most suitable model, and the dataset with the highest R^2 value was selected for further feature selection and model improvement. Molecular docking studies demonstrated that compound 15j had a strong binding affinity toward α -glucosidase, with a docking score of -10.04 kcal/mol, and formed several remarkable interactions, particularly three key hydrogen bonds with TYR158, GLN353, and GLU411, contributing to its high inhibitory efficacy. The results of the molecular dynamics simulation demonstrated that the 15j- α -glucosidase complex exhibits high stability and effectively maintains its binding without causing significant structural changes in the enzyme, confirming the stable interaction and selective inhibition of this compound at the enzyme's active site.

Keywords [1,2,4]Triazolo[1,5-*a*]pyridine, α -Glucosidase, α -Amylase, Machine learning model

^{1,2,4}Triazolo[1,5-*a*]pyridines are significant fused aza-heterocyclic compounds present in some well-known drugs, such as Filgotinib (as an oral, selective inhibitor of Janus kinase 1 (JAK1)), Tucatinib (as tyrosine kinase inhibitor to target HER2), and Enarodustat (as an oral hypoxia-inducible factor prolyl hydroxylase (HIF-PH) inhibitor). Among various derivatives of this scaffold, ones bearing 8-cyano moiety have been proved to exhibit diverse remarkable pharmacological activities, including anti-inflammatory and antioxidant^{1,2}, antibacterial^{3,4}, antifungal^{5,6}, adenosine receptor antagonists⁷, potent and orally bioavailable roryt inverse agonist⁸, PDE10A inhibitors⁹, immunomodulators¹⁰, and as the key intermediate to afford negative allosteric modulators of mGlu5¹¹. In addition to medicinal applications, these compounds have shown potential in high-performance organic light-emitting diodes (OLEDs) due to their outstanding deep-blue emission and stability¹². Although

¹Department of Medicinal Chemistry, Faculty of Pharmacy, Tehran University of Medical Sciences, Tehran, Iran.

²Drug Design and Development Research Center, The Institute of Pharmaceutical Sciences (TIPS), Tehran University of Medical Sciences, Tehran, Iran. ³International Campus-School of Pharmacy, Tehran University of Medical Sciences, Tehran, Iran. ⁴Faculty of Pharmacy, Eastern Mediterranean University, via Mersin 10, Famagusta, TRNC, Turkey. ⁵The Engineered Biomaterials Research Center, Khazar University, Baku, Azerbaijan. ⁶Faculty of Pharmacy, Final International University, Kyrenia via Mersin 10 Turkey, Catalkoy, TRNC, Turkey. ⁷Department of Pharmaceutical Biotechnology, Faculty of Pharmacy, Tehran University of Medical Sciences, Tehran, Iran. ⁸Department of Bioinformatics and Systems Biology, School of Advanced Technologies in Medicine, Isfahan University of Medical Sciences, Isfahan, Iran. ⁹Department of Toxicology and Pharmacology, Faculty of Pharmacy and Toxicology and Diseases Group, Pharmaceutical Sciences Research Center (PSRC), The Institute of Pharmaceutical Sciences (TIPS), Tehran University of Medical Sciences, Tehran, Iran. ✉email: firoozpour@gmail.com; aforoumadi@yahoo.com

numerous applications of ^{1,2,4}triazolo[1,5-*a*]pyridine-8-carbonitriles have been reported to date, its α -glucosidase inhibitory potential has not yet been investigated.

The α -glucosidase enzyme plays a crucial role in carbohydrate metabolism, primarily functioning in the epithelium of the small intestine, where it hydrolyzes complex carbohydrates into absorbable glucose. By catalyzing this final step in carbohydrate digestion, it directly influences postprandial blood glucose levels. Inhibiting α -glucosidase activity delays carbohydrate breakdown, resulted into reducing glucose absorption to the bloodstream and helping to manage hyperglycemia effectively. Already, one of the most pivotal approved approaches for the treatment of type 2 diabetes mellitus (T2DM) and its resultant postprandial hyperglycemia is the inhibition of α -glucosidase. Although its inhibitors such as acarbose and miglitol have been widely used in clinical settings to treat diabetes, these agents are associated with limitations, including gastrointestinal side effects, and limited efficacy. The most commonly reported adverse effects of α -glucosidase inhibitors include abdominal discomfort such as flatulence, diarrhea, and stomach pain¹³. Despite remarkable advancements in diabetes treatment and the development of novel therapeutic strategies, the global burden of diabetes remains a significant challenge^{14,15}. To address this growing health crisis, numerous compounds as potential α -glucosidase inhibitors with enhanced efficacy and improved safety profiles have been reported within recent decade^{16–21}.

As a part of our continuing research about potential α -glucosidase inhibitors^{22–27}, herein we present a straightforward synthetic route to afford novel poly-substituted ^{1,2,4}triazolo[1,5-*a*]pyridine-8-carbonitriles **15**, to evaluate their potency to inhibit this enzyme. In recent years, triazoles have gained considerable attention as prominent pharmacophores in chemical biology and drug discovery. Their distinctive structural features enable the formation of crucial protein–ligand interactions, such as hydrogen bonds and π – π stacking, have made them as valuable scaffold targeting a wide range of therapeutic pathways^{28–37}. Additionally, extensive studies have highlighted the significance of triazole-based scaffolds, whether 1,2,3- or 1,2,4-triazoles, linked with or fused to other nitrogen-containing heterocycles, as valuable structures for designing α -glucosidase inhibitors. A variety of molecular hybrids, including pyridazine-triazole, pyrazoline-triazole, benzothiazole-triazole, benzimidazole-triazole, quinazolinone-triazole, thiazolo-triazole, and indole-triazole, have exhibited notable antidiabetic activity through inhibition of α -glucosidase³⁸. To the best of our knowledge, the α -glucosidase inhibitory activity of the ^{1,2,4}triazolopyridine scaffold has not yet been investigated. Therefore, we synthesized a series of novel derivatives based on this scaffold to complement the current understanding of fused triazole systems as potential α -glucosidase inhibitors.

So far, various synthetic approaches for the preparation of ^{1,2,4}triazolo[1,5-*a*]pyridine-8-carbonitriles have been reported in the literature. One of them involved using substituted 3-(1,2,4-triazol-5-yl)acetonitriles which went through the condensation with β -dicarbonyl compounds^{5,39,40} or α,β -unsaturated nitriles and esters^{41–43}. In present study, this synthon underwent the Michael-addition-cyclocondensation with α -azidochalcones to afford the targeted compounds. Notably, α -azidochalcones have gained considerable attention in recent decade in organic synthesis for their utility in constructing a variety of nitrogen-containing heterocycles^{44–54}.

In present study, an efficient strategy was employed to prepare a wide range of 6-amino-2,5,7-triaryl-^{1,2,4}triazolo[1,5-*a*]pyridine-8-carbonitriles **15a–15v**. Subsequently, all of the synthesized compounds were evaluated in α -glucosidase inhibition assessment, revealing their remarkable inhibitory potencies, with IC₅₀ values ranging from 6.60 ± 0.09 μ M to 75.63 ± 0.44 μ M, in comparison with acarbose as a positive control (750.00 ± 0.56 μ M). Compound **15j** emerged as the most potent inhibitor, being approximately 98-fold greater potency than the standard drug. Consequently, further assessments, including α -amylase inhibition, kinetic study, and comprehensive computational studies (machine learning models, molecular docking studies, and molecular dynamics simulations) were conducted to provide insights into the binding interactions and inhibitory mechanisms of the synthesized compounds, with compound **15j** showing stable and strong binding within the active site of α -glucosidase.

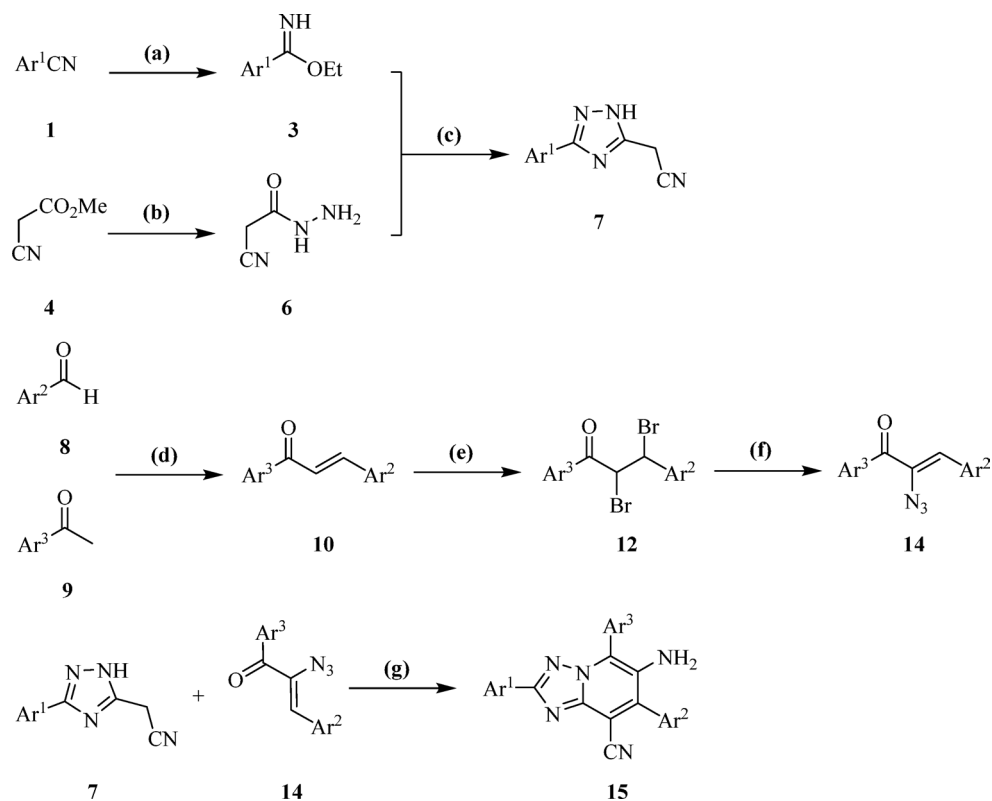
Results and discussion

Chemistry

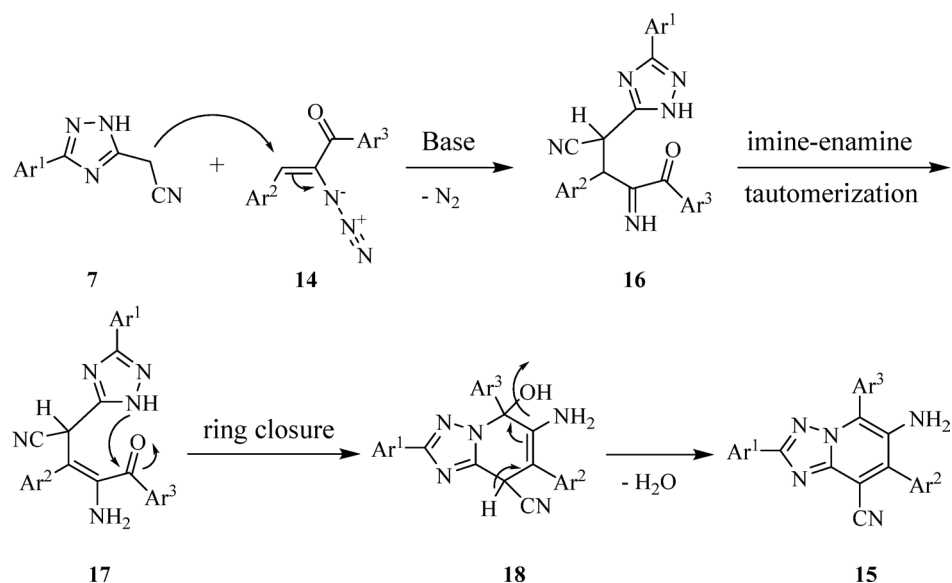
The general procedure to afford the targeted 6-amino-2,5,7-triaryl-^{1,2,4}triazolo[1,5-*a*]pyridine-8-carbonitriles **15** is outlined in Scheme 1. As illustrated, The synthesis involved two key precursors: 3-aryl-(1,2,4-triazol-5-yl)acetonitriles **7** and substituted α -azidochalcones **14**, which were prepared through separate pathways. The synthetic route to obtain 3-aryl-(1,2,4-triazol-5-yl)acetonitriles **7** was initiated through the Pinner reaction between substituted benzonitriles **1** and absolute ethanol **2** in the presence of acyl chloride to give adduct **3**, followed by the cyclization with 2-cyanoacetohydrazide **6**, which itself was produced from the efficient condensation of methyl 2-cyanoacetate **4** with an excess of hydrazine hydrate **5**.

On the other hand, the protocol to prepare the adduct **14** involved three steps: initially, a condensation reaction between arylaldehyde **8** and 1-(aryl)ethan-1-one **9** in basic conditions produced the corresponding chalcone **10**. This intermediate then went through the bromination of olefin (compound **12**), followed by the nucleophilic substitution using sodium azide **13**, resulting in the desired substituted α -azidochalcones **14**.

Finally, a Michael-addition-cyclocondensation proceeded between 3-aryl-(1,2,4-triazol-5-yl)acetonitriles **7** and α -azidochalcones **14** to afford the targeted poly-substituted triazolopyridines **15a–15v**. These reactions were carried out different conditions to study the role of additives, solvents, reactions conditions, and time. This led us to perform the reaction in the presence of potassium carbonate in ethanol under the reflux conditions within 2 h to afford the targeted triazolopyridines within the highest yields. In our procedure, ethanol was chosen as the solvent due to its moderate polarity, protic nature, and ability to dissolve both organic and inorganic reactants efficiently, which facilitated better interaction between substrates and enhanced the reaction rate. Moreover, ethanol's polarity stabilized the intermediate species and thus favored the formation of the desired triazolopyridine products with high selectivity. Potassium carbonate was employed as a good base to activate the nucleophilic sites and facilitate the cyclization process, thereby improving the overall yield of the products.



Scheme 1. Reaction conditions and reagents: (a) substituted benzonitriles **1**, absolute EtOH **2**, AcCl, r.t., 4 h; (b) hydrazine hydrate **3**, neat, r.t., 1 h; (c) Et₃N, EtOH, reflux, 12 h; (d) NaOH, H₂O, EtOH, r.t., 3 h; (e) Br₂ **11**, Et₂O, r.t., 4 h; (f) NaN₃ **13**, DMF, r.t., 3 h; (g) K₂CO₃, EtOH, reflux, 2 h.



Scheme 2. Proposed reaction mechanism.

The structures of all isolated products were completely deduced on the basis of their IR, ¹H and ¹³C NMR spectroscopy, high-resolution mass spectrometry (HRMS), and elemental analysis. Partial assignments of these resonances are given in the Experimental Part.

A reasonable mechanism for the formation of 6-amino-2,5,7-triaryl-1,2,4-triazolo[1,5-*a*]pyridine-8-carbonitriles **15** is depicted in Scheme 2. The reaction may be initiated by the base-activated nucleophilic Michael addition of 3-aryl-(1,2,4-triazol-5-yl)acetone nitriles **7** from C-atom to the α -azido chalcones **14**, followed

by removal of a nitrogen molecule to give intermediate **16**. Subsequently, this adduct may undergo an imine-enamine tautomerization (intermediate **17**) and cyclocondensation reaction of the N-atom of triazole ring and the adjacent carbonyl group to close the triazolo[1,5-*a*]pyridine skeleton (intermediate **18**). Finally, dehydration yields the desired product **15**.

α -Glucosidase inhibitory activity

As desirable 6-amino-2,5,7-triaryl-^{1,2,4}triazolo[1,5-*a*]pyridine-8-carbonitriles **15a–15v** were successfully synthesized, their *in vitro* inhibitory potencies against α -glucosidase (extracted from *Saccharomyces cerevisiae*) were evaluated, and the results were compared with Acarbose as the reference drug. As summarized in Table 1, all compounds exhibited great to excellent inhibitory activities (ranging from $6.60 \pm 0.09 \mu\text{M}$ to $75.63 \pm 0.44 \mu\text{M}$), which were several times superior than that of acarbose with IC_{50} value of $750.00 \pm 0.56 \mu\text{M}$.

Initially, the Ar^1 was remained as unsubstituted phenyl ring to investigate the role of substituents on the Ar^2 and Ar^3 rings. To explain the structure and observed activity correlations, poly-substituted triazolopyridines **15a–t** were divided into four categories considering the substituents on the Ar^2 ring: (1) unsubstituted derivatives **15a–15g**; (2) 4-methylphenyl derivatives **15h–15L**; (3) 4-methoxyphenyl derivatives **15m–15p**; (4) 4-chlorophenyl derivatives **15q–15t**. In each series, several substituents on Ar^3 were also altered to optimize the α -glucosidase inhibition. Subsequently, compounds **15u** and **15v** were synthesized to investigate the role of substituents on the Ar^1 ring.

In the first series, compound **15a** showed a notable inhibitory activity with an IC_{50} value of $20.32 \pm 0.11 \mu\text{M}$. Introducing chlorine group at C-4 position of Ar^3 significantly increased the potency (compound **15c**, $\text{IC}_{50} = 9.69 \pm 0.09 \mu\text{M}$), which demonstrated the strongest activity within this series. However, introducing this atom at other positions, substituting bromine and methoxy at C-4 position of this phenyl (compounds **15b**, **15d–15f**), or replacing this phenyl with thiophene (compound **15g**) caused detrimental effect on inhibition potency.

About the second series, the introduction of methyl at C-4 position of Ar^2 in compound **15h** in comparison with **15a** enhanced the α -glucosidase inhibition ($\text{IC}_{50} = 14.37 \pm 0.43 \mu\text{M}$). The introduction of whether methoxy or chlorine at C-4 position of Ar^3 led to further improvement on the potency, as compounds **15i** and **15j** possessed the IC_{50} values of $8.43 \pm 0.25 \mu\text{M}$ and $6.60 \pm 0.09 \mu\text{M}$, respectively. It is worth mentioning compound **15j** emerged as the most potent derivative in this study and demonstrated approximately 98-fold superior than that acarbose. Same as previous category, the presence of bromine at C-4 position (compound **15k**) and the incorporation of phenyl with thiophene (compound **15l**) resulted in a significant deterioration in activity.

Across third and fourth categories, compounds followed similar activity trends as their analogs in the first series. Investigating the role of substituent on Ar^1 revealed that introducing a methoxy group on Ar^1 enhanced α -glucosidase inhibition compared to the unsubstituted derivative (compound **15u**, $\text{IC}_{50} = 14.78 \pm 0.22 \mu\text{M}$, vs. compound **15a**, $\text{IC}_{50} = 20.32 \pm 0.11 \mu\text{M}$). In contrast, the presence of a chlorine atom on this ring led to a reduction in inhibitory activity (compound **15v**, $25.13 \pm 0.24 \mu\text{M}$).

The SAR analysis revealed that the presence of electron-donating groups, such as methyl and methoxy, on Ar^2 was beneficial for α -glucosidase inhibition, while the presence of electron-withdrawing group, chlorine or bromine, was detrimental for activity. Compounds with an unsubstituted phenyl ring on Ar^2 showed moderate inhibitory effects. For the Ar^3 ring, the presence of chlorine atom at C-4 position notably improved potency against α -glucosidase across all series. An unsubstituted phenyl was also beneficial inhibitory activity; while other alterations on Ar^3 caused a decrease in α -glucosidase inhibition. Regarding Ar^1 , the introduction of methoxy group improved the inhibitory activity. Based on the insights gained about substituents on the Ar^2 and Ar^3 rings, our future studies will explore the effects of introducing various groups at different positions on the Ar^3 ring to further optimize activity. Figure 1 presents an overall SAR trend overview.

The α -glucosidase inhibition assessments on the triazolopyridines **15a–15v** led us to opt 6-amino-5-(4-chlorophenyl)-2-phenyl-7-(*p*-tolyl)-^{1,2,4}triazolo[1,5-*a*]pyridine-8-carbonitrile **15j**, the most pivotal inhibitor in present study, as potential candidate for further evaluations.

α -Amylase inhibitory activity

Although triazolopyridine **15j** exhibited remarkable α -glucosidase inhibitory activity, it showed no α -amylase inhibition. Acarbose was used as the control drug in this study, showing the $50.1 \pm 0.5\%$ inhibition. This selectivity is of particular importance because α -glucosidase plays a direct role in the final step of carbohydrate digestion, converting disaccharides into glucose, which is readily absorbed into the bloodstream. By selectively targeting α -glucosidase, the compound effectively delays glucose absorption and mitigates postprandial hyperglycemia without interfering with the earlier stages of carbohydrate digestion mediated by α -amylase. Such selectivity leads to reduce common gastrointestinal side effects, such as bloating and gas, which are often associated with non-specific inhibition of both enzymes.

The lack of α -amylase inhibition ensures the preservation of normal starch digestion, reducing the potential for gastrointestinal discomfort and malabsorption. This targeted mechanism of action highlights the potential of the triazolopyridine **15j** as a promising candidate for the development of antidiabetic therapies. By focusing on α -glucosidase inhibition, the compound **15j** offers a more precise approach to glycemic control, addressing a critical aspect of diabetes management while minimizing off-target effects. These results highlighted the importance of developing enzyme-specific inhibitors to improve the efficacy and safety profiles of therapeutic agents.

The low IC_{50} value of **15j** suggests that its structural features are highly favorable for binding to α -glucosidase, likely due to an optimal combination of ring systems, functional groups, and molecular geometry that enhance its interaction with the enzyme's active site. However, some compounds, such as acarbose and gallic acid, act as dual inhibitors of both α -amylase and α -glucosidase. Acarbose, due to its intramolecular nitrogen, binds to

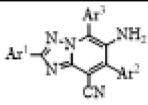
				
Compound	Ar ¹	Ar ²	Ar ³	IC ₅₀ (μM) ^a
15a				20.32 ± 0.11
15b				25.50 ± 0.23
15c				9.69 ± 0.09
15d				45.54 ± 0.25
15e				60.64 ± 0.18
15f				31.97 ± 0.32
15g				45.73 ± 0.29
15h				14.37 ± 0.43
15i				8.43 ± 0.25
15j				6.60 ± 0.09
15k				29.89 ± 0.17
15l				21.49 ± 0.09
15m				9.18 ± 0.12
15n				22.31 ± 0.08
15o				7.64 ± 0.13
15p				36.33 ± 0.09
15q				38.18 ± 0.14
15r				49.96 ± 0.11
15s				31.49 ± 0.08
15t				75.63 ± 0.44
15u				14.78 ± 0.22
15v				25.13 ± 0.24
Acarbose	—	—	—	750.00 ± 0.56

Table 1. Substrate scope and in vitro α -glucosidase inhibitory activity of targeted 6-amino-2,5,7-triaryl-1,2,4-triazolo[1,5-*a*]pyridine-8-carbonitriles **15a–15v**.

^aValues are expressed as mean \pm SD. All experiments were performed at least three times.

the carbohydrate recognition site of α -glucosidase with greater affinity than its natural substrate⁵⁵. Similarly, many polyphenolic compounds, such as flavonoids and gallic acid, exhibit inhibitory effects on both α -amylase and α -glucosidase, making them broad-spectrum carbohydrate digestion inhibitors. While some compounds lack selectivity, others exhibit distinct inhibition mechanisms. For example, aurone derivatives containing phenylureido or bis-phenylureido moieties inhibit both α -glucosidase and α -amylase, but through different mechanisms. Rather than directly blocking substrate binding, aurone derivatives interact with a hydrophilic allosteric site in α -amylase, located far from the active site at the N-terminal⁵⁶. Compared to these inhibitors, triazolopyridine **15j** demonstrated remarkable selectivity for α -glucosidase over α -amylase, suggesting that its

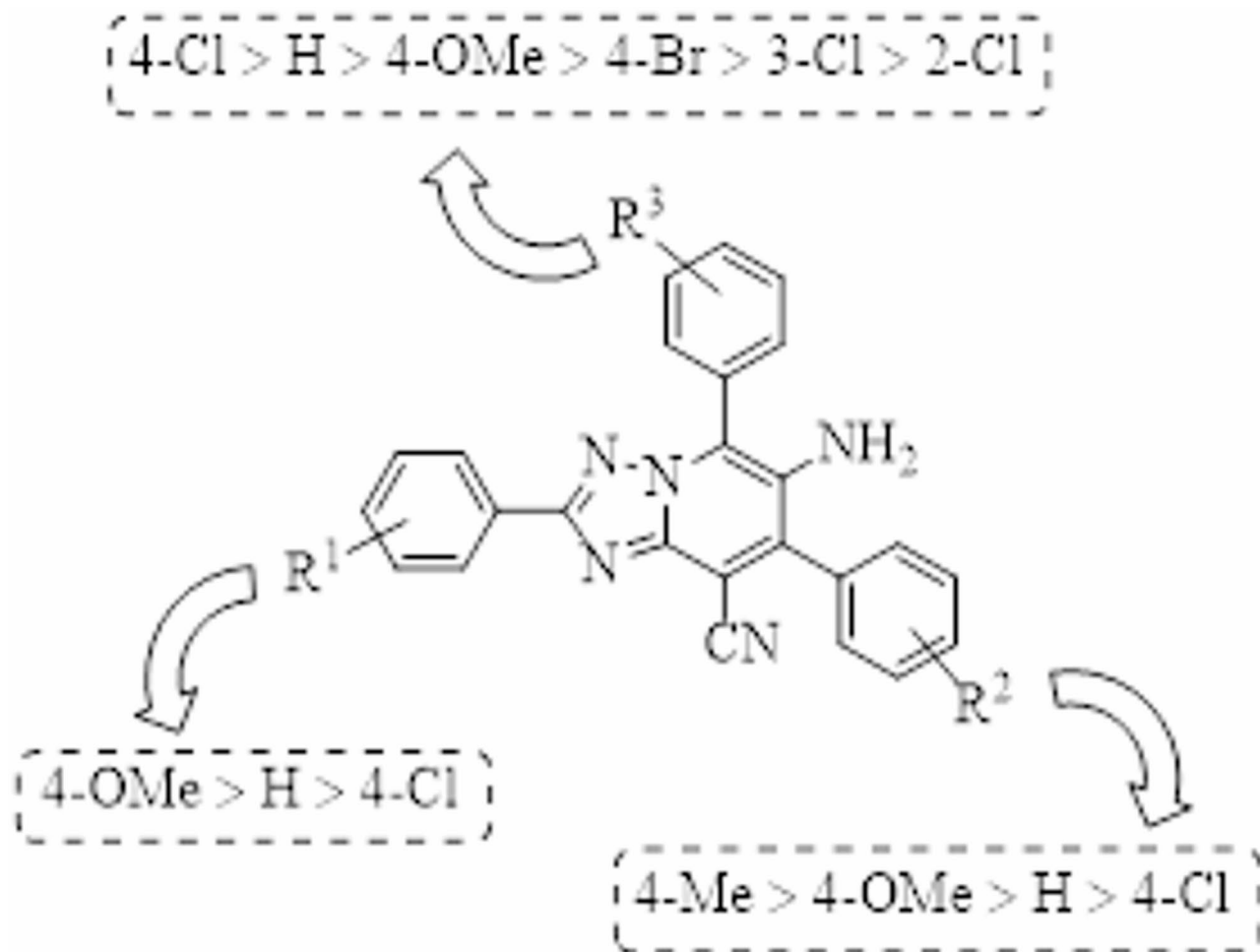


Fig. 1. The summary of SAR trend.

molecular structure is specifically optimized for α -glucosidase binding while minimizing off-target interactions with α -amylase. This high selectivity makes **15j** a promising candidate for targeted therapeutic applications, particularly in conditions where specific α -glucosidase inhibition is desired without affecting α -amylase activity.

Enzyme kinetic studies

Kinetic study was performed to identify the α -glucosidase inhibition mode of poly-substituted 1,2,4-triazolo[1,5-*a*]pyridine **15j**. The inhibition assessment was proceeded using different concentrations of p-nitrophenyl α -D-glucopyranoside (1–16 mM) as the substrate, both in the absence and presence of various concentrations of compound **15j** (0, 1.6, 3.3, and 6.6 μ M). Across the relationship between the concentration of substrate and the rate of reaction, kinetic studies lead researchers to determine key parameters such as the Michaelis-Menten constant (K_m) and the maximum velocity (V_{max}). This information is vital for characterizing the type of inhibition, which can be classified as competitive, non-competitive, or uncompetitive, thus providing insights into the mechanism of action for potential inhibitors.

Accordingly, a Lineweaver-Burk plot was outlined to determine the V_{max} and K_m values. As depicted in Fig. 2, increasing the inhibitor concentration resulted in an increase in the K_m value, while the V_{max} remained unchanged. This observation indicates a competitive inhibition mechanism, where triazolopyridine **15j** competes with the substrate for binding to the active site of α -glucosidase. To determine the inhibitor's binding affinity, K_m values were plotted against different concentrations of compound **15j** (Fig. 2B), and this analysis estimated the inhibition constant (K_i) to be 6.6 μ M.

The effect of triazolopyridine **15j** on the kinetics parameters of α -glucosidase (Michaelis-Menten equation parameters (V_{max} , K_m , K_i)) are presented in Table 2.

Computational studies

In this study, comprehensive computational studies, including machine learning modeling, molecular docking, and molecular dynamic simulation, were employed to provide accurate insight about the biological activities and interactions of desirable 6-amino-2,5,7-triaryl-1,2,4-triazolo[1,5-*a*]pyridine-8-carbonitriles **15a–15v**.

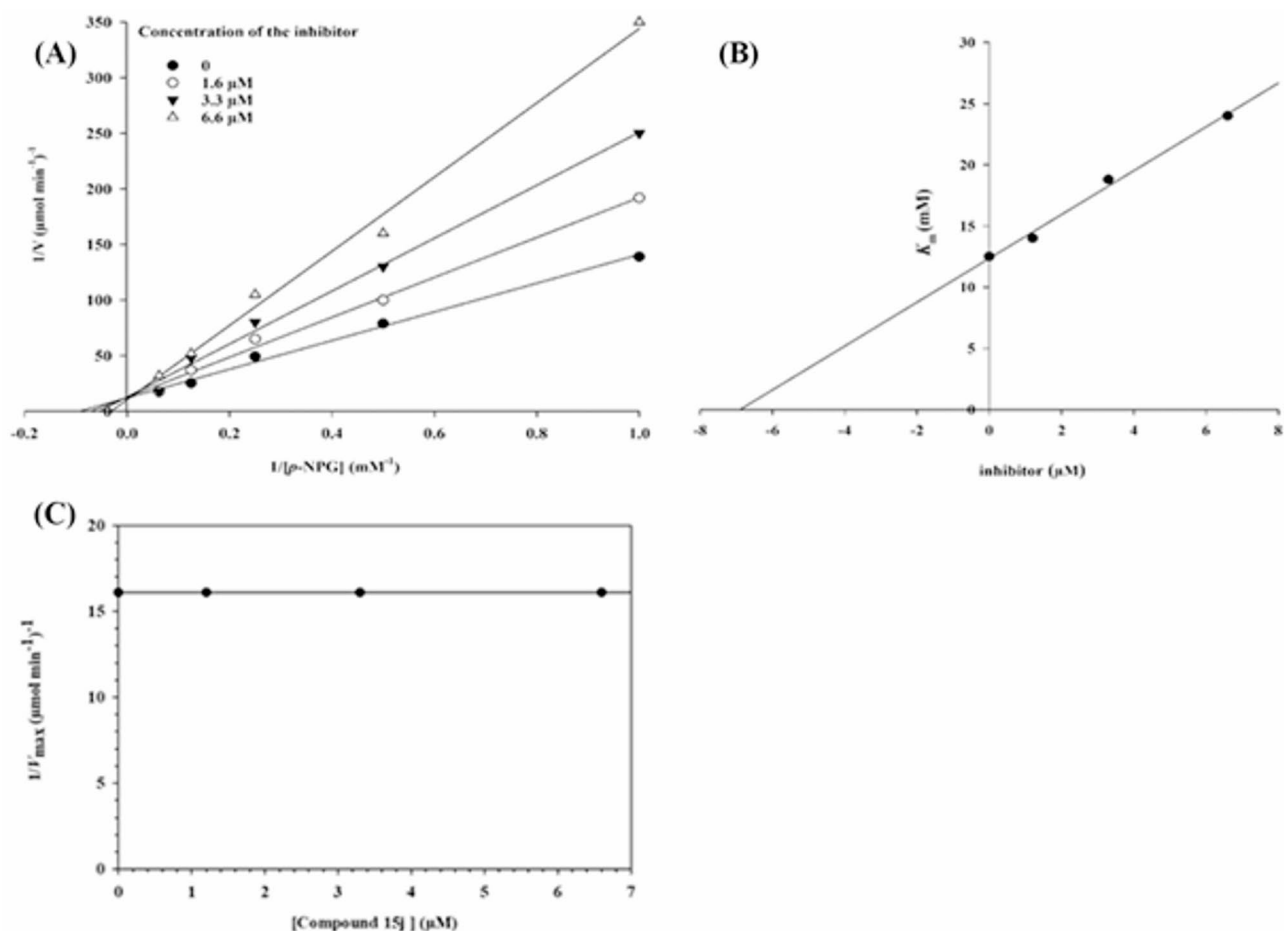


Fig. 2. Kinetics study about α -glucosidase inhibition by compound 15j: (A) the Lineweaver–Burk plot in the absence and presence of different concentrations of the inhibitor; (B) the secondary plot between K_m and various concentrations of the inhibitor; (C) the plot of $1/V_{\text{max}}$ vs. inhibitor concentration.

Sample	Michaelis–Menten constant (K_m)	Maximum velocity (V_m)	Inhibition constant (K_i)
Untreated α -glucosidase	12.5 mM	62.5 (nmol min^{-1})	–
The enzyme treated with 6.6 μM compound 15j	24.0 mM	62.5 (nmol min^{-1})	6.6 μM

Table 2. Kinetic parameters in this study.

Machine learning modeling

Quantitative Structure-Activity Relationship (QSAR) analysis is a computer-aided drug design tool using machine learning to predict the biological activity of novel compounds based on the reported chemical structures against various biological targets. In current study, a broad library containing 1477 compounds was prepared and docked with protein PDB ID of 3A4A to identify the optimal interaction patterns with α -glucosidase, and the machine-learning algorithm used in this QSAR study was tree-based regression models, as one of powerful and popular tools in this context⁵⁷.

Tree-based regression models, including Random Forest, Extra Trees, and LightGBM, were trained on the seven conformer collections generated from the docking studies. The performance of each model was assessed using squared correlation scores across the collections to determine the optimal model and the most informative fingerprint vectors. As illustrated in Fig. 3, three heatmaps display the R^2 scores of regression models applied to the seven conformer collections. These heatmaps highlight variations in model performance, with certain collections demonstrating superior predictive power. Among the collections, Glide_evdw achieved the highest performance across all three models. For instance, the Random Forest algorithm consistently exhibited high R^2 scores for most collections, showing its strong predictive capability for this dataset. Based on the heatmap analysis, Random Forest was identified as the most suitable model, and the dataset with the highest R^2 value was selected for further feature selection and model improvement.

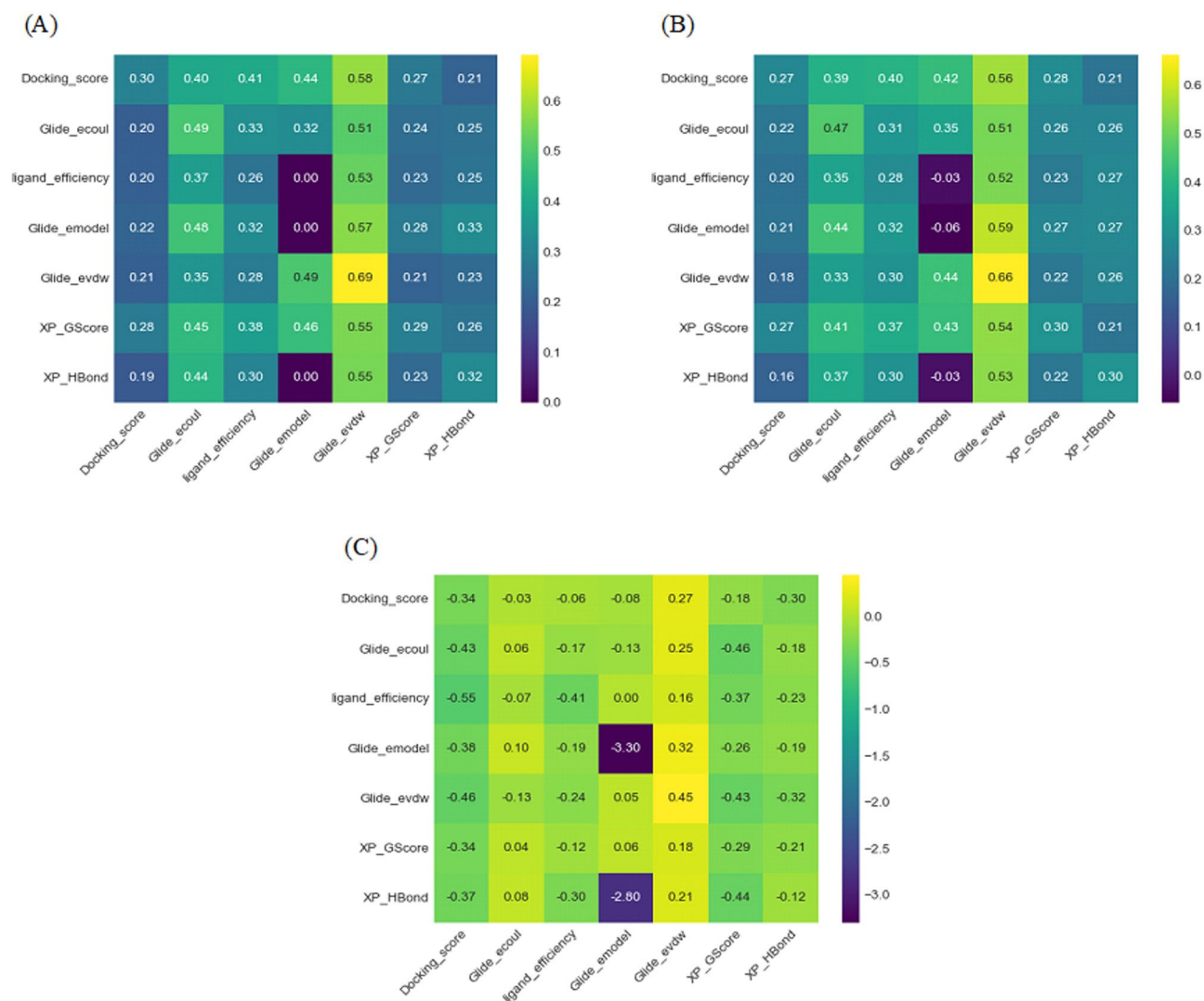


Fig. 3. Heatmaps of R^2 scores for the (A) Random Forest; (B) LightGBM; (C) Extra Trees, models across seven conformer collections.

A variety of fingerprint vectors were utilized to train the Random Forest model and estimate inhibition levels. Figure 4 presents the ROC plot comparing these fingerprints, indicating that the AUC values did not differ significantly among the various types. Consequently, the ‘Estate’ fingerprints were selected for further analysis. These fingerprints represent molecular structures as binary vectors that record the presence or absence of specific substructures within a molecule, making them highly effective for similarity searches and predictive modeling.

Although the study attempted to evaluate the direct effect of interactional fingerprints on model performance, no significant improvement was observed over structural fingerprints. Therefore, structural fingerprints remain the preferred choice in this context.

With the Estate fingerprint achieving an AUC score of 0.65, the model was employed to predict the inhibitory activity of newly synthesized compounds **15a–15v**. As shown in Table 3, the model successfully predicted the activity of these compounds, highlighting its practical utility in designing and identifying further potential α -glucosidase inhibitors.

Molecular docking studies

The molecular docking studies performed with the Glide software from Schrödinger Suite 14.0 on α -glucosidase (PDB ID: 3A4A) revealed valuable insights into the binding affinities and interaction patterns of the studied compounds. As summarized in Table 3, the docking scores, indicative of binding affinity, ranged from -8.63 to -10.41 kcal/mol, highlighting the strong binding affinity of the 6-amino-2,5,7-triaryl-^{1,2,4}triazolo[1,5-*a*]pyridine-8-carbonitriles **15a–15v**.

Among the compounds, two derivatives with better inhibitory potency (compounds **15j** and **15o**) are shown in Fig. 5. As depicted, the key residues involved in ligand interactions, including ASP307, ARG315, TYR158, and PHE303, playing pivotal roles within the enzyme’s active site. Several remarkable interactions, particularly

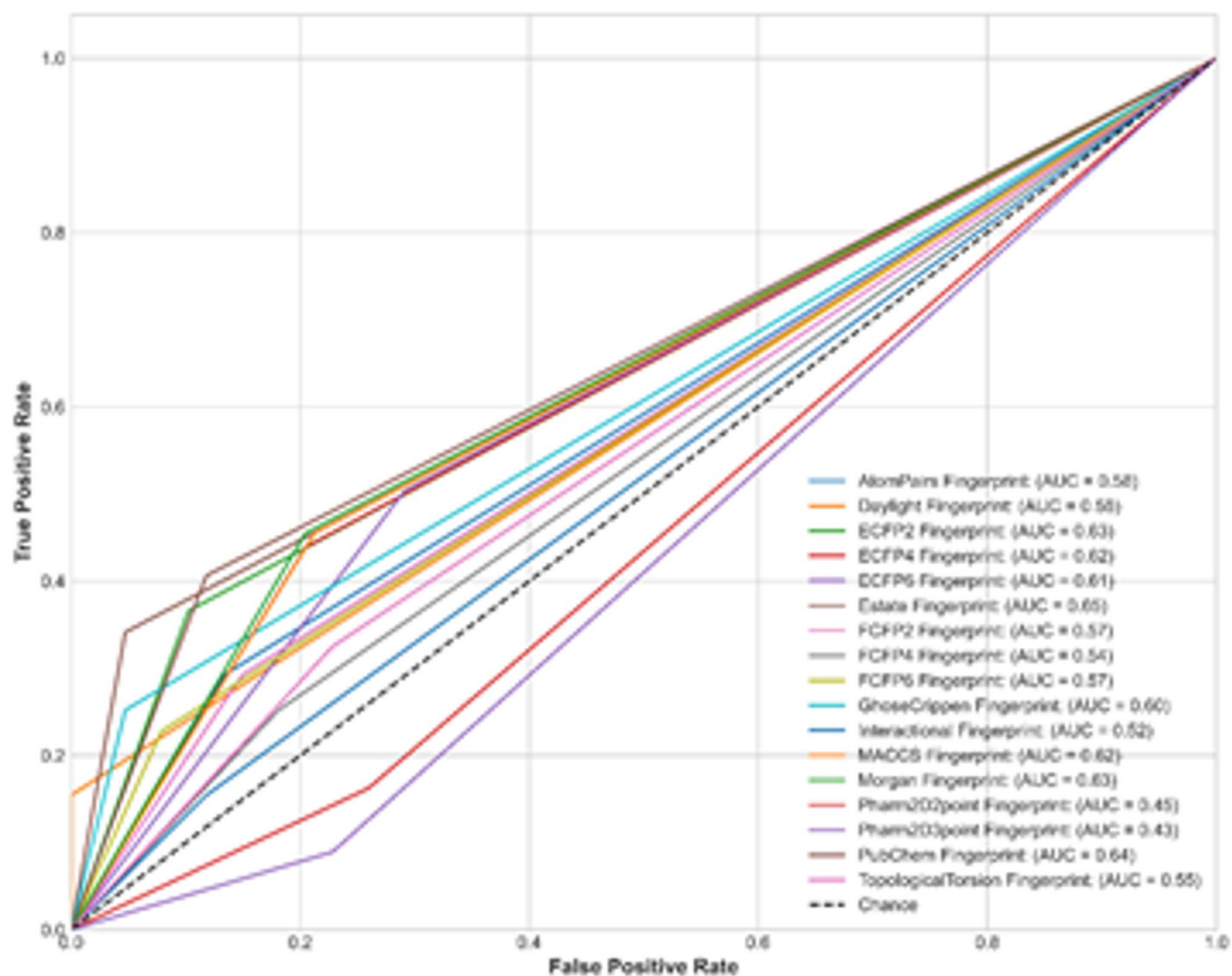


Fig. 4. ROC plot comparing the performance of various molecular fingerprint types using the Random Forest classification model.

hydrogen bonding, were identified as a primary stabilizing force in the ligand-receptor complex. Among the compounds, triazolopyridine **15j** emerged as the most potent, with an IC_{50} value of 6.60 μ M, forming three hydrogen bonds with residues TYR158, GLN353, and GLU411, which contributed to its strong binding affinity and superior inhibitory efficacy. Additionally, triazolopyridine **15o** demonstrated lower docking score (-10.34 kcal/mol), featuring a Pi-Pi stacking interaction with PHE303. This interaction, along with its favorable docking score, confirmed its excellent binding potency.

Molecular dynamic simulation

Molecular dynamics (MD) simulation is essential in α -glucosidase inhibition studies, as it presents the structural and functional dynamics of enzyme-ligand interactions. By simulating the interaction of the enzyme and its inhibitors, researchers can visualize binding mechanisms and conformational changes at an atomic level; therefore, they can determine the key residues that influence binding affinity. Additionally, MD evaluates the stability of the inhibitor-enzyme complex through parameters like Root Mean Square Deviation (RMSD), enabling the distinction between competitive and non-competitive inhibition mechanisms.

MD simulations were conducted on the most potent inhibitory triazolopyridine, **15j**, to further analyze its stability and binding interactions with α -glucosidase. Using the Desmond module of the Schrödinger Suite, the **15j**- α -glucosidase complex was simulated for 200 ns in an explicit solvent environment. The system was equilibrated under physiological conditions, and periodic boundary conditions were applied to mimic a continuous system. The primary goal of the simulation was to evaluate the stability of **15j**'s binding pose within the enzyme's active site and to observe the dynamic behavior of key interacting residues. Figure 6 demonstrated the RMSD plot of compound **15j** in the α -glucosidase complex over the 200 ns simulation. The triazolopyridine **15j** complex (green line) maintained significantly lower RMSD values compared to the acarbose complex (blue line) throughout the simulation, particularly stabilizing around 2.5 Å. This indicates that compound **15j** effectively retained its binding conformation during the MD simulation. Additionally, the RMSD of this

Label	IC ₅₀ (μM)	Dock score (kcal/mol)	count inhibitor prediction	Residue	Interaction type
15a	20.32 ± 0.11	- 9.33	10	ASP307	H-Bonding
15b	25.50 ± 0.23	- 9.52	8	ASP233	H-Bonding
15c	9.69 ± 0.09	- 9.47	10	ASP307	H-Bonding
15d	45.54 ± 0.25	- 9.47	10	ASP307	H-Bonding
15e	60.64 ± 0.18	- 9.46	10	ASP307 ARG315	H-Bonding Halogen-Bond
15f	31.97 ± 0.32	- 9.46	8	ASP307	H-Bonding
15g	45.73 ± 0.29	- 9.05	10	ASP307	H-Bonding
15h	14.37 ± 0.43	- 9.91	10	ASP307	H-Bonding
15i	8.43 ± 0.25	- 10.10	3	HIE280	Pi-Pi stacking
15j	6.60 ± 0.09	- 10.04	10	TYR158 GLN353 GLU411	H-Bonding H-Bonding H-Bonding
15k	29.89 ± 0.17	- 10.06	10	-	-
15L	21.49 ± 0.09	- 9.78	10	TYR158 HIE280	Pi-Pi stacking Pi-Pi stacking
15m	9.18 ± 0.12	- 10.20	8	ARG315 ASN415	Pi-cation H-Bonding
15n	22.31 ± 0.08	- 10.41	2	-	-
15o	7.64 ± 0.13	- 10.34	7	PHE303	Pi-Pi stacking
15p	36.33 ± 0.09	- 10.04	8	PHE303 ASP307	Pi-Pi stacking H-Bonding
15q	38.18 ± 0.14	- 9.92	10	ARG315 ASN415	Pi-cation H-Bonding
15r	49.96 ± 0.11	- 10.04	7	LYS156 TYR158	H-Bonding Pi-Pi stacking
15s	31.49 ± 0.08	- 9.99	10	ASP233 LYS432	H-Bonding Pi-cation
15t	75.63 ± 0.44	- 9.69	10	ASN415	H-Bonding
15u	14.78 ± 0.22	- 8.63	8	ASP307 ARG315	H-Bonding Pi-cation
15v	25.13 ± 0.24	- 8.78	10	ASP307 ARG315	H-Bonding Pi-cation

Table 3. Predicted inhibitory activity of newly synthesized 6-amino-2,5,7-triaryl-1,2,4-triazolo[1,5-*a*]pyridine-8-carbonitriles **15a–15v** as potential α-glucosidase inhibitors using the estate fingerprint model.

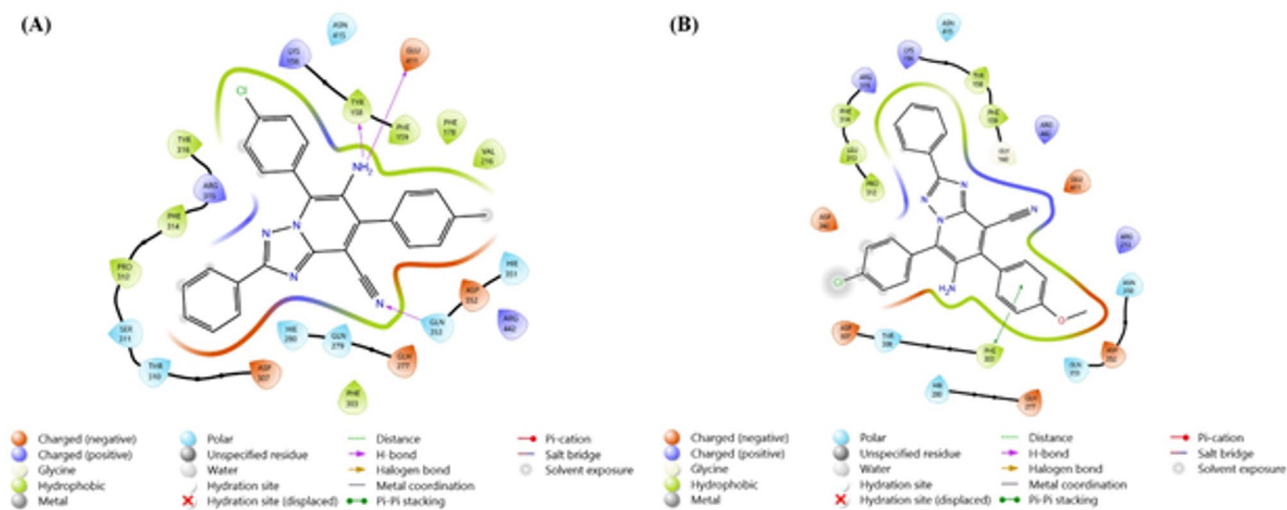


Fig. 5. Docking interaction profile of (A) compound **15j**; (B) compound **15o**.

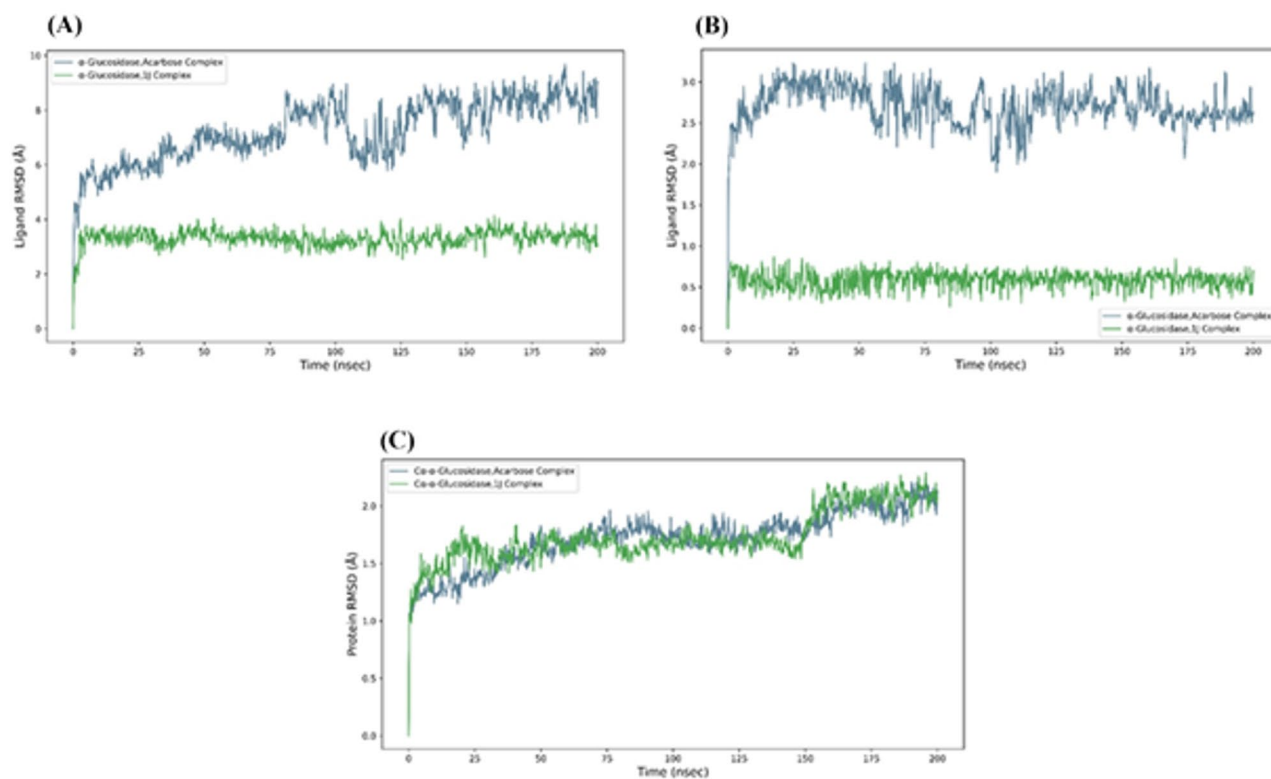


Fig. 6. (A) Lig_wrt_Protein: RMSD of the ligand relative to the whole protein complex; (B) Lig_wrt_Ligand: The RMSD of the ligand with respect to its own initial or reference conformation, in which the movement of the protein does not interfere; (C) Prot_CA: RMSD of Ca atoms of α -glucosidase in two complexes.

triazolopyridine remained below 1.0 Å after initial equilibration, with no substantial deviation from its bound state, suggesting a highly stable interaction within the enzyme's active site.

In Fig. 6C, the Ca RMSD of both the α -glucosidase–acarbose complex (blue line) and the α -glucosidase–15j complex (green line) stabilized after the initial equilibration phase, fluctuating between 1.5 and 2.0 Å. The similar RMSD profiles for both complexes indicate that binding of either ligand does not cause significant structural changes in the protein over the simulation time frame.

The calculated binding free energies (MM/GBSA) indicate that compound 15j exhibited a lower average binding free energy (-50.50 ± 4.69 kcal/mol) compared to acarbose (-33.83 ± 7.97 kcal/mol). These results suggest a stronger and more stable interaction of compound 15j within the α -glucosidase active site, supporting its enhanced inhibitory potency.

Conclusion

Given the necessity of discovering novel α -glucosidase inhibitor scaffolds, a series of 6-amino-2,5,7-triaryl-1,2,4-triazolo[1,5-*a*]pyridine-8-carbonitriles **15a–15v** was successfully synthesized and evaluated for their inhibitory activities. These compounds exhibited excellent to strong α -glucosidase inhibition, with IC_{50} values ranging from 6.60 ± 0.09 μ M to 75.63 ± 0.44 μ M, significantly more potent than the reference drug acarbose ($IC_{50} = 750.00 \pm 0.56$ μ M). Among them, compound 15j emerged as the most potent and selective α -glucosidase inhibitor, with no detectable α -amylase inhibition. Kinetic studies revealed that 15j inhibits α -glucosidase through a competitive mechanism by binding to the enzyme's active site.

In silico studies also supported these findings. The machine learning model, trained with the Estate fingerprint, achieved an AUC score of 0.65, demonstrating its utility in predicting α -glucosidase inhibition. One of the main limitations in our QSAR model is the low structural diversity of the molecular database because the compounds only differ primarily with benzene-based substitutions. This kind of structural homology reduces the power of the model to capture more subtle variations of substituent effects. The molecular fingerprints utilized may also not be able to identify these subtle variations, thus affecting predictive accuracy. Future improvements can include more advanced molecular representations, i.e., natural language processing (NLP)-based descriptors or molecular graph approaches, that can better capture the nuanced effects of changing substituents and enhance model performance. Molecular docking studies revealed strong hydrogen bonding interactions of compound 15j with key residues TYR158, GLN353, and GLU411. Additionally, molecular dynamics simulations confirmed the stability of the 15j-enzyme complex, validating its potential as a promising lead compound for further development of α -glucosidase inhibitors.

Experimental

All chemicals were purchased from Merck (Germany) and were used without further purification. The reaction progress and the purity of synthesized compounds were monitored by thin-layer chromatography (TLC) on silica gel 250-micron F254 plastic sheets; zones were detected visually under UV light (254 nm). Melting points were measured on an Electrothermal 9100 apparatus. IR spectra were recorded on a Shimadzu IR-460 spectrometer. ^1H and ^{13}C NMR spectra were measured (DMSO- d_6 solution) with Bruker DRX-500 AVANCE (at 500.1 and 125.1 MHz) and Bruker DRX-300 AVANCE (at 300.1 and 75.1 MHz) instruments. Chemical shifts were reported in parts per million (ppm), downfield from tetramethylsilane. Proton coupling patterns were described as singlet (s), doublet (d), triplet (t), and multiplet (m). HRMS analysis was performed using a Waters Synapt G1 HDMS High Definition mass spectrometer equipped with an electrospray ionization (ESI) source. The samples were prepared by diluting the isolated compounds in methanol to a final concentration of 10 $\mu\text{g}/\text{mL}$. The analysis was conducted in negative ion mode with a mass range of m/z 50–1000. Elemental analyses for C, H, and N were performed using a Heraeus CHN-O-Rapid analyzer.

General synthetic procedures

General procedure for the Preparation of substituted Ethyl benzimidates 7

To a stirring solution of substituted benzonitrile **1** (1 equiv.) and absolute ethanol **2** (12 equiv.) under the ice bath conditions at 0 °C, acetyl chloride (8 equiv.) was added dropwise. The reaction vessel was then tightly sealed, and stirring continued for 4 h. Upon completion of the reaction, as monitored by TLC, the reaction mixture was cooled to 0 °C, gradually neutralized with saturated aqueous NaHCO_3 , and extracted with Et_2O three times. The organic layer was then washed with brine, dried over Na_2SO_4 , concentrated under reduced pressure. The residue was finally purified by the column chromatography using *n*-hexane/ EtOAc (7:3) as the eluent to afford the pure imidate **3** as colorless liquids (yield: 63–78%)⁵⁸.

General procedure for the preparation of 2-cyanoacetohydrazide 6

Methyl 2-cyanoacetate **4** (1 equiv.) was stirred at room temperature in a balloon, and hydrazine hydrate **5** (2 equiv.) was gradually added over time. Stirring was maintained for one hour until white solids began to form. After completing the reaction, the resulting precipitate was isolated through filtration, thoroughly washed with methanol and water, and dried to give pure 2-cyanoacetohydrazide **6** (yield: 90%)⁵⁹.

General procedure for the preparation of 3-aryl-(1,2,4-triazol-5-yl)acetonitriles 7

A mixture of substituted ethyl benzimidate **3** (1 equiv.), 2-cyanoacetohydrazide **6** (1 equiv.), and triethylamine (1.5 equiv.) in ethanol was stirred under the reflux conditions for 12 h. Upon completion of the reaction as confirmed by TLC, the reaction mixture was diluted with cool water, resulting in the formation of white precipitate. Finally, the crude product was filtered off and recrystallized from acetonitrile to afford the pure products **7** (yield: 75–88%)³⁹.

General procedure for the preparation of chalcones 10

To a stirring solution of NaOH (1 equiv.) in EtOH and water under the ice bath conditions at 0 °C, 1-(aryl)ethan-1-ones **9** (1 equiv.) was added to get activated. After 5 min, aldehyde **8** (1 equiv.) was introduced to the solution, and temperature increased suddenly up to 30 °C. The reaction proceeded for 3 h until completion. Afterwards, the mixture was transferred to the refrigerator within 10 h. The resulting precipitate was filtered and washed with a mixture of cold water and EtOH to yield pure corresponding chalcone **10** (yield: 72–88%).

General procedure for the preparation of dibromochalcones 12

To the stirring solution of chalcone **10** (1 equiv.) in ether under the ice bath conditions at 0 °C, bromine (Br_2) **11** (1.2 equiv.) was added drop by drop, and reaction proceeded at this temperature for 4 h. As the mixture got pale, the reaction completion was confirmed by TLC analysis. Subsequently, the mixture was poured into cold water to precipitate. As solid product formed, it was filtered and thoroughly washed with water. The desired compound **12** was sufficiently pure for subsequent steps without the need for any further purification processes (yield: 82–90%).

General procedure for the preparation of α -azidochalcones 14

A mixture of dibromochalcone **12** (1 equiv.) and sodium azide (NaN_3) **13** (4 equiv.) in DMF at ambient temperature within the appropriate time until the starting materials finished. Afterwards, the mixture was poured into water to extract three times with EtOAc . The combined organic phases were washed with brine, dried over Na_2SO_4 , and then concentrated. The residue was crystallized from *n*-Hexane to give the pure, corresponding α -azidochalcones **14** (yield: 70–84%)⁴⁶.

General procedure for the preparation of 6-amino-2,5,7-triaryl-1,2,4-triazolo[1,5-a]pyridine-8-carbonitriles 15

To a stirring solution of 3-aryl-(1,2,4-triazol-5-yl)acetonitriles **7** (1 equiv.) and K_2CO_3 (2 equiv.) in EtOH at room temperature, corresponding α -azidochalcone **14** (1 equiv.) was added gradually, and the reaction mixture was then heated under the reflux conditions for 2 h. As the completion of reaction was confirmed, the mixture was cooled to the room temperature, leading to the precipitation of the desired product. The powder was filtered and washed thoroughly with sufficient amount of Et_2O to yield pure poly-substituted triazolopyridines **15** as pale-yellow solids (yield: 58–90%).

6-Amino-2,5,7-triphenyl-1,2,4-triazolo[1,5-a]pyridine-8-carbonitrile (15a) Pale-yellow solid, mp 184–187 °C, yield: 78%. IR (KBr) ($\nu_{\text{max}}/\text{cm}^{-1}$): 3390 and 3323 (NH_2), 2237 ($\text{C}\equiv\text{N}$), 1571, 1511, 1449, 1258, 1225, 1152, 1122,

1094, 1025, 951, 916, 853, 803, 802, 750, 689, 665. ^1H NMR (500.1 MHz, DMSO- d_6): δ 8.22 (d, $J=7.9$ Hz, 2 H, 2CH), 8.05 (d, $J=7.8$ Hz, 2 H, 2CH), 8.01 (d, $J=8.2$ Hz, 2 H, 2CH), 7.88 (t, $J=7.4$ Hz, 1H, CH), 7.77 (t, $J=7.0$ Hz, 2 H, 2CH), 7.69–7.52 (m, 5 H, 5CH), 7.45 (t, $J=7.4$ Hz, 1H, CH), 4.16 (s, 2 H, NH_2). ^{13}C NMR (125.1 MHz, DMSO- d_6): δ 153.87, 145.49, 140.64, 136.37, 136.05, 134.46, 133.97, 131.69, 130.83, 130.20, 130.10, 129.73, 129.70, 126.69, 124.89, 123.47, 118.02, 114.30, 97.46. HRMS (ESI) m/z for $\text{C}_{25}\text{H}_{16}\text{N}_5^-$ [M - H] $^-$, calculated: 386.1411, found: 386.1398. Anal. Calcd. for $\text{C}_{25}\text{H}_{17}\text{N}_5$: C, 77.50; H, 4.42; N, 18.08; found: C, 77.68; H, 4.29; N, 18.33%.

6-Amino-5-(4-methoxyphenyl)-2,7-diphenyl-1,2,4-triazolo[1,5-*a*]pyridine-8-carbonitrile (15b) Pale-yellow solid, mp 203–205 °C, yield: 76%. IR (KBr) ($\nu_{\text{max}}/\text{cm}^{-1}$): 3348 and 3250 (NH_2), 2251 ($\text{C}\equiv\text{N}$), 1557, 1538, 1502, 1443, 1355, 1236, 1178, 1027, 833, 751, 665. ^1H NMR (500.1 MHz, DMSO- d_6): δ 8.17 (d, $J=8.0$ Hz, 2 H, 2CH), 8.04–7.94 (m, 4 H, 4CH), 7.76–7.46 (m, 5 H, 5CH), 7.40 (t, $J=7.5$ Hz, 1H, CH), 7.25 (d, $J=8.8$ Hz, 2 H, 2CH), 4.21 (s, 2 H, NH_2), 3.87 (s, 3 H, OCH_3). ^{13}C NMR (125.1 MHz, DMSO- d_6): δ 164.25, 153.70, 145.30, 140.52, 135.94, 134.34, 134.08, 133.32, 131.42, 130.52, 129.99, 129.59, 126.58, 124.95, 123.36, 117.84, 115.00, 114.18, 97.35, 56.64. HRMS (ESI) m/z for $\text{C}_{26}\text{H}_{18}\text{N}_5\text{O}^-$ [M - H] $^-$, calculated: 416.1517, found: 416.1536. Anal. Calcd. for $\text{C}_{26}\text{H}_{19}\text{N}_5\text{O}$: C, 74.80; H, 4.59; N, 16.78; found: C, 74.96; H, 4.80; N, 16.96%.

6-Amino-5-(4-chlorophenyl)-2,7-diphenyl-1,2,4-triazolo[1,5-*a*]pyridine-8-carbonitrile (15c) Pale-yellow solid, mp 219–222 °C, yield: 90%. IR (KBr) ($\nu_{\text{max}}/\text{cm}^{-1}$): 3328 and 3224 (NH_2), 2214 ($\text{C}\equiv\text{N}$), 1565, 1539, 1501, 1448, 1420, 1309, 1233, 1189, 1124, 1002, 979, 927, 839, 750, 691, 659. ^1H NMR (500.1 MHz, DMSO- d_6): δ 8.24 (d, $J=7.8$ Hz, 2 H, 2CH), 8.07 (dd, $J=7.6$, 1.9 Hz, 2 H, 2CH), 8.04 (d, $J=8.6$ Hz, 2 H, 2CH), 7.84 (d, $J=8.6$ Hz, 2 H, 2CH), 7.70–7.54 (m, 5 H, 5CH), 7.47 (t, $J=7.2$ Hz, 1H, CH), 4.32 (s, 2 H, NH_2). ^{13}C NMR (125.1 MHz, DMSO- d_6): δ 153.92, 145.57, 140.70, 138.43, 136.13, 135.67, 133.91, 132.29, 131.34, 130.54, 129.97, 129.36, 129.26, 126.77, 124.64, 123.56, 117.12, 114.37, 97.54. HRMS (ESI) m/z for $\text{C}_{25}\text{H}_{15}\text{ClN}_5^-$ [M - H] $^-$, calculated: 420.1021, found: 420.1048. Anal. Calcd. for $\text{C}_{25}\text{H}_{16}\text{ClN}_5$: C, 71.17; H, 3.82; N, 16.60; found: C, 70.98; H, 3.94; N, 16.67%.

6-Amino-5-(3-chlorophenyl)-2,7-diphenyl-1,2,4-triazolo[1,5-*a*]pyridine-8-carbonitrile (15d) Pale-yellow solid, mp 191–193 °C, yield: 69%. IR (KBr) ($\nu_{\text{max}}/\text{cm}^{-1}$): 3325 and 3257 (NH_2), 2239 ($\text{C}\equiv\text{N}$), 1550, 1534, 1478, 1435, 1353, 1319, 1249, 1102, 943, 888, 795, 751, 679, 652. ^1H NMR (500.1 MHz, DMSO- d_6): δ 8.28 (d, $J=8.1$ Hz, 2 H, 2CH), 8.20 (s, 1H, CH), 8.10–8.00 (m, 3 H, 3CH), 7.94 (t, $J=7.5$ Hz, 1H, CH), 7.80 (t, $J=7.8$ Hz, 2 H, 2CH), 7.72–7.62 (m, 4 H, 4CH), 7.50 (t, $J=7.6$ Hz, 1H, CH), 4.37 (s, 2 H, NH_2). ^{13}C NMR (125.1 MHz, DMSO- d_6): δ 154.19, 145.99, 140.90, 137.33, 136.44, 136.34, 135.97, 131.78, 131.30, 131.11, 130.67, 130.49, 130.40, 128.06, 126.99, 124.51, 123.78, 117.86, 114.59, 97.76. HRMS (ESI) m/z for $\text{C}_{25}\text{H}_{15}\text{ClN}_5^-$ [M - H] $^-$, calculated: 420.1021, found: 420.0994. Anal. Calcd. for $\text{C}_{25}\text{H}_{16}\text{ClN}_5$: C, 71.17; H, 3.82; N, 16.60; found: C, 71.01; H, 3.99; N, 16.51%.

6-Amino-5-(2-chlorophenyl)-2,7-diphenyl-1,2,4-triazolo[1,5-*a*]pyridine-8-carbonitrile (15e) Pale-yellow solid, mp 178–179 °C, yield: 61%. IR (KBr) ($\nu_{\text{max}}/\text{cm}^{-1}$): 3296 and 3238 (NH_2), 2240 ($\text{C}\equiv\text{N}$), 1568, 1534, 1499, 1446, 1399, 1352, 1251, 1223, 1143, 1053, 889, 797, 750, 696, 658. ^1H NMR (500.1 MHz, DMSO- d_6): δ 8.47 (dd, $J=7.8$, 1.9 Hz, 1H, CH), 8.22 (d, $J=8.3$ Hz, 2 H, 2CH), 8.06 (d, $J=8.2$ Hz, 2 H, 2CH), 7.91 (t, $J=7.4$ Hz, 1H, CH), 7.80 (t, $J=7.7$ Hz, 2 H, 2CH), 7.73 (d, $J=7.8$ Hz, 1H, CH), 7.70–7.55 (m, 4 H, 4CH), 7.46 (t, $J=7.4$ Hz, 1H, CH), 4.31 (s, 2 H, NH_2). ^{13}C NMR (125.1 MHz, DMSO- d_6): δ 153.90, 145.69, 140.64, 137.04, 136.46, 136.01, 134.21, 132.12, 131.84, 130.93, 130.71, 130.10, 129.66, 128.42, 126.68, 124.66, 124.27, 123.47, 118.55, 114.30, 97.46. HRMS (ESI) m/z for $\text{C}_{25}\text{H}_{15}\text{ClN}_5^-$ [M - H] $^-$, calculated: 420.1021, found: 420.1032. Anal. Calcd. for $\text{C}_{25}\text{H}_{16}\text{ClN}_5$: C, 71.17; H, 3.82; N, 16.60; found: C, 71.25; H, 3.73; N, 16.79%.

6-Amino-5-(4-bromophenyl)-2,7-diphenyl-1,2,4-triazolo[1,5-*a*]pyridine-8-carbonitrile (15f) Pale-yellow solid, mp 246–249 °C, yield: 89%. IR (KBr) ($\nu_{\text{max}}/\text{cm}^{-1}$): 3298 and 3159 (NH_2), 2219 ($\text{C}\equiv\text{N}$), 1554, 1533, 1475, 1437, 1354, 1303, 1154, 1100, 950, 879, 816, 780, 750, 676. ^1H NMR (500.1 MHz, DMSO- d_6): δ 8.25 (d, $J=7.9$ Hz, 2 H, 2CH), 8.10 (d, $J=8.3$ Hz, 2 H, 2CH), 8.01 (d, $J=8.6$ Hz, 2 H, 2CH), 7.97 (d, $J=8.6$ Hz, 2 H, 2CH), 7.72–7.56 (m, 5 H, 5CH), 7.48 (t, $J=7.3$ Hz, 1H, CH), 4.40 (s, 2 H, NH_2). ^{13}C NMR (125.1 MHz, DMSO- d_6): δ 154.11, 145.76, 140.89, 136.74, 136.32, 134.31, 133.14, 133.00, 132.04, 130.65, 130.38, 129.99, 128.16, 126.96, 124.40, 123.73, 117.52, 114.57, 97.73. HRMS (ESI) m/z for $\text{C}_{25}\text{H}_{15}\text{BrN}_5^-$ [M - H] $^-$, calculated: 464.0516, found: 464.0538. Anal. Calcd. for $\text{C}_{25}\text{H}_{16}\text{BrN}_5$: C, 64.39; H, 3.46; N, 15.02; found: C, 64.48; H, 3.29; N, 15.26%.

6-Amino-2,7-diphenyl-5-(thiophen-2-yl)-1,2,4-triazolo[1,5-*a*]pyridine-8-carbonitrile (15 g) Pale-yellow solid, mp 177–179 °C, yield: 74%. IR (KBr) ($\nu_{\text{max}}/\text{cm}^{-1}$): 3326 and 3224 (NH_2), 2236 ($\text{C}\equiv\text{N}$), 1583, 1531, 1440, 1353, 1120, 1079, 926, 839, 802, 755, 708, 662. ^1H NMR (500.1 MHz, DMSO- d_6): δ 8.37 (dd, $J=4.9$, 1.1 Hz, 1H, CH), 8.25 (d, $J=7.9$ Hz, 2 H, 2CH), 8.18–8.09 (m, 3 H, 3CH), 7.72–7.58 (m, 5 H, 5CH), 7.53 (t, $J=4.4$ Hz, 1H, CH), 7.47 (t, $J=7.1$ Hz, 1H, CH), 4.23 (s, 2 H, NH_2). ^{13}C NMR (125.1 MHz, DMSO- d_6): δ 152.53, 145.98, 141.70, 140.54, 137.27, 136.96, 136.22, 134.10, 131.62, 130.02, 129.87, 129.61, 127.98, 126.61, 123.39, 122.61, 113.71, 112.40, 95.78. HRMS (ESI) m/z for $\text{C}_{23}\text{H}_{14}\text{N}_5\text{S}^-$ [M - H] $^-$, calculated: 392.0975, found: 392.0998. Anal. Calcd. for $\text{C}_{23}\text{H}_{15}\text{N}_5\text{S}$: C, 71.75; H, 3.85; N, 16.73; found: C, 71.62; H, 3.92; N, 16.90%.

6-Amino-2,5-diphenyl-7-(*p*-tolyl)-1,2,4-triazolo[1,5-*a*]pyridine-8-carbonitrile (15 h) Pale-yellow solid, mp 188–190 °C, yield: 64%. IR (KBr) ($\nu_{\text{max}}/\text{cm}^{-1}$): 3319 and 3221 (NH_2), 2224 ($\text{C}\equiv\text{N}$), 1551, 1534, 1458, 1432, 1353, 1312, 1278, 1200, 1151, 1078, 1039, 950, 850, 751, 689. ^1H NMR (300.1 MHz, DMSO- d_6): δ 8.22 (d, $J=8.2$ Hz, 2 H, 2CH), 7.94 (d, $J=7.9$ Hz, 2 H, 2CH), 7.87 (d, $J=7.6$ Hz, 2 H, 2CH), 7.78–7.68 (m, 3 H, 3CH), 7.63 (t, $J=7.8$ Hz, 2 H, 2CH), 7.53 (d, $J=7.9$ Hz, 2 H, 2CH), 7.38 (t, $J=7.3$ Hz, 1H, CH), 4.14 (s, 2 H, NH_2), 2.28 (s, 3 H, CH_3). ^{13}C NMR (75.1 MHz, DMSO- d_6): δ 153.76, 145.65, 139.85, 136.12, 135.01, 133.61, 132.56, 131.72,

130.50, 130.11, 129.76, 129.71, 129.10, 126.33, 124.61, 123.62, 117.87, 114.46, 97.54, 21.71. HRMS (ESI) m/z for $C_{27}H_{20}N_5O^- [M - H]^-$, calculated: 400.1568, found: 400.1592. Anal. Calcd. for $C_{27}H_{21}N_5O$: C, 75.16; H, 4.91; N, 16.23; found: C, 75.23; H, 5.12; N, 16.38%.

6-Amino-5-(4-methoxyphenyl)-2-phenyl-7-(p-tolyl)-1,2,4-triazolo[1,5-a]pyridine-8-carbonitrile (15i) Pale-yellow solid, mp 206–209 °C, yield: 72%. IR (KBr) ($\nu_{\max}/\text{cm}^{-1}$): 3303 and 3100 (NH_2), 2244 ($\text{C}\equiv\text{N}$), 1532, 1473, 1446, 1381, 1356, 1287, 1134, 1100, 1026, 950, 884, 821, 752, 719, 660. ^1H NMR (500.1 MHz, $\text{DMSO}-d_6$): δ 8.22 (d, $J=7.7$ Hz, 2 H, 2CH), 8.00 (d, $J=8.5$ Hz, 2 H, 2CH), 7.94 (d, $J=7.9$ Hz, 2 H, 2CH), 7.63 (t, $J=8.1$ Hz, 2 H, 2CH), 7.46–7.40 (m, 3 H, 3CH), 7.29 (d, $J=7.9$ Hz, 2 H, 2CH), 4.34 (s, 2 H, NH_2), 3.36 (s, 3 H, OCH_3), 2.32 (s, 3 H, CH_3). ^{13}C NMR (125.1 MHz, $\text{DMSO}-d_6$): δ 164.32, 153.89, 145.49, 140.75, 140.71, 136.04, 133.38, 131.67, 131.51, 130.41, 130.18, 129.72, 126.76, 124.30, 123.55, 117.68, 115.15, 114.39, 97.44, 56.04, 21.19. HRMS (ESI) m/z for $C_{26}H_{18}N_5^- [M - H]^-$, calculated: 430.1673, found: 430.1704. Anal. Calcd. for $C_{26}H_{19}N_5$: C, 77.79; H, 4.77; N, 17.44; found: C, 77.91; H, 4.64; N, 17.52%.

6-Amino-5-(4-chlorophenyl)-2-phenyl-7-(p-tolyl)-1,2,4-triazolo[1,5-a]pyridine-8-carbonitrile (15j) Pale-yellow solid, mp 222–224 °C, yield: 86%. IR (KBr) ($\nu_{\max}/\text{cm}^{-1}$): 3319 and 3175 (NH_2), 2223 ($\text{C}\equiv\text{N}$), 1536, 1501, 1449, 1402, 1326, 1251, 1200, 1179, 1121, 1028, 983, 927, 870, 823, 794, 701, 670. ^1H NMR (500.1 MHz, $\text{DMSO}-d_6$): δ 8.31 (dd, $J=8.5, 1.0$ Hz, 2 H, 2CH), 8.07 (d, $J=8.5$ Hz, 2 H, 2CH), 8.05 (d, $J=8.2$ Hz, 2 H, 2CH), 7.90 (d, $J=8.5$ Hz, 2 H, 2CH), 7.71 (t, $J=7.9$ Hz, 2 H, 2CH), 7.58–7.48 (m, 3 H, 3CH), 4.30 (s, 2 H, NH_2), 2.32 (s, 3 H, CH_3). ^{13}C NMR (125.1 MHz, $\text{DMSO}-d_6$): δ 154.04, 145.69, 141.34, 140.84, 138.84, 136.49, 136.16, 133.78, 132.84, 132.05, 130.57, 130.31, 129.98, 126.89, 124.08, 123.67, 117.26, 114.50, 97.58, 21.23. HRMS (ESI) m/z for $C_{26}H_{17}ClN_5^- [M - H]^-$, calculated: 434.1178, found: 434.1136. Anal. Calcd. for $C_{26}H_{18}ClN_5$: C, 71.64; H, 4.16; N, 16.07; found: C, 71.78; H, 4.23; N, 15.88%.

6-Amino-5-(4-bromophenyl)-2-phenyl-7-(p-tolyl)-1,2,4-triazolo[1,5-a]pyridine-8-carbonitrile (15k) Pale-yellow solid, mp 256–259 °C, yield: 90%. IR (KBr) ($\nu_{\max}/\text{cm}^{-1}$): 3337 and 3202 (NH_2), 2254 ($\text{C}\equiv\text{N}$), 1521, 1475, 1439, 1397, 1333, 1254, 1222, 1178, 1026, 999, 956, 861, 833, 750, 695. ^1H NMR (500.1 MHz, $\text{DMSO}-d_6$): δ 8.29 (d, $J=8.2$ Hz, 2 H, 2CH), 8.08–8.00 (m, 4 H, 4CH), 7.98 (d, $J=8.5$ Hz, 2 H, 2CH), 7.70 (t, $J=7.8$ Hz, 2 H, 2CH), 7.59–7.46 (m, 3 H, 3CH), 4.45 (s, 2 H, NH_2), 2.32 (s, 3 H, CH_3). ^{13}C NMR (125.1 MHz, $\text{DMSO}-d_6$): δ 154.17, 145.73, 141.38, 140.87, 136.87, 136.21, 133.80, 132.98, 132.95, 132.10, 130.60, 130.34, 127.95, 126.92, 124.51, 123.70, 117.42, 114.54, 97.62, 21.81. HRMS (ESI) m/z for $C_{26}H_{17}BrN_5^- [M - H]^-$, calculated: 478.0673, found: 478.0702. Anal. Calcd. for $C_{26}H_{18}BrN_5$: C, 65.01; H, 3.78; N, 14.58; found: C, 65.14; H, 3.83; N, 14.76%.

6-Amino-2-phenyl-5-(thiophen-2-yl)-7-(p-tolyl)-1,2,4-triazolo[1,5-a]pyridine-8-carbonitrile (15 L) Pale-yellow solid, mp 183–185 °C, yield: 74%. IR (KBr) ($\nu_{\max}/\text{cm}^{-1}$): 3350 and 3250 (NH_2), 2241 ($\text{C}\equiv\text{N}$), 1551, 1518, 1472, 1440, 1372, 1346, 1250, 1166, 1092, 997, 977, 829, 841, 809, 751, 682, 648. ^1H NMR (500.1 MHz, $\text{DMSO}-d_6$): δ 8.37 (d, $J=4.9$ Hz, 1H, CH), 8.26 (d, $J=7.8$ Hz, 2 H, 2CH), 8.12 (d, $J=3.8$ Hz, 1H, CH), 8.05 (d, $J=8.1$ Hz, 2 H, 2CH), 7.67 (t, $J=7.9$ Hz, 2 H, 2CH), 7.54 (t, $J=4.4$ Hz, 1H, CH), 7.52–7.45 (m, 3 H, 3CH), 4.38 (s, 2 H, NH_2), 2.33 (s, 3 H, CH_3). ^{13}C NMR (125.1 MHz, $\text{DMSO}-d_6$): δ 153.62, 145.07, 141.82, 140.80, 140.60, 137.07, 136.74, 136.00, 133.21, 131.74, 130.29, 130.07, 129.85, 126.66, 124.14, 123.44, 116.71, 112.45, 95.74, 21.36. HRMS (ESI) m/z for $C_{24}H_{16}N_5S^- [M - H]^-$, calculated: 406.1132, found: 406.1154. Anal. Calcd. for $C_{24}H_{17}N_5S$: C, 70.74; H, 4.20; N, 17.19; found: C, 70.85; H, 4.02; N, 17.25%.

6-Amino-7-(4-methoxyphenyl)-2,5-diphenyl-1,2,4-triazolo[1,5-a]pyridine-8-carbonitrile (15 m) Pale yellow solid, mp 191–193 °C, yield: 69%. IR (KBr) ($\nu_{\max}/\text{cm}^{-1}$): 3336 and 3292 (NH_2), 2227 ($\text{C}\equiv\text{N}$), 1591, 1541, 1467, 1418, 1325, 1225, 1126, 1075, 1032, 958, 854, 818, 779, 720, 667. ^1H NMR (500.1 MHz, $\text{DMSO}-d_6$): δ 8.18 (d, $J=7.7$ Hz, 2 H, 2CH), 7.98 (d, $J=8.8$ Hz, 2 H, 2CH), 7.90 (d, $J=7.4$ Hz, 2 H, 2CH), 7.81 (t, $J=7.5$ Hz, 1H, CH), 7.70 (t, $J=7.9$ Hz, 2 H, 2CH), 7.57 (t, $J=7.8$ Hz, 2 H, 2CH), 7.39 (t, $J=7.4$ Hz, 1H, CH), 7.12 (d, $J=8.8$ Hz, 2 H, 2CH), 4.34 (s, 2 H, NH_2), 3.79 (s, 3 H, OCH_3). ^{13}C NMR (125.1 MHz, $\text{DMSO}-d_6$): δ 161.58, 153.74, 145.46, 140.54, 137.66, 135.97, 133.66, 130.98, 130.51, 130.01, 129.57, 126.60, 126.54, 124.98, 123.37, 117.82, 115.17, 114.20, 97.31, 55.62. HRMS (ESI) m/z for $C_{26}H_{18}N_5O^- [M - H]^-$, calculated: 416.1517, found: 416.1498. Anal. Calcd. for $C_{26}H_{19}N_5O$: C, 74.80; H, 4.59; N, 16.78; found: C, 74.74; H, 4.64; N, 16.62%.

6-Amino-5,7-bis(4-methoxyphenyl)-2-phenyl-1,2,4-triazolo[1,5-a]pyridine-8-carbonitrile (15n) Pale yellow solid, mp 220–223 °C, yield: 78%. IR (KBr) ($\nu_{\max}/\text{cm}^{-1}$): 3373 and 3249 (NH_2), 2251 ($\text{C}\equiv\text{N}$), 1531, 1494, 1414, 1382, 1301, 1250, 1201, 1121, 1026, 1000, 825, 790, 750, 700, 648. ^1H NMR (500.1 MHz, $\text{DMSO}-d_6$): δ 8.16 (dd, $J=8.5, 0.9$ Hz, 2 H, 2CH), 8.05 (d, $J=7.9$ Hz, 2 H, 2CH), 8.03 (d, $J=7.8$ Hz, 2 H, 2CH), 7.56 (t, $J=8.0$ Hz, 2 H, 2CH), 7.38 (t, $J=7.2$ Hz, 1H, CH), 7.22 (d, $J=7.8$ Hz, 2 H, 2CH), 7.11 (d, $J=7.9$ Hz, 2 H, 2CH), 4.39 (s, 2 H, NH_2), 3.79 and 3.81 (2s, 6 H, 2 OCH_3). ^{13}C NMR (125.1 MHz, $\text{DMSO}-d_6$): δ 163.94, 161.27, 153.65, 145.30, 140.47, 135.91, 133.37, 133.03, 129.94, 129.35, 126.63, 126.52, 124.80, 123.31, 117.64, 115.05, 114.89, 114.44, 97.24, 55.84, 55.25. HRMS (ESI) m/z for $C_{27}H_{20}N_5O_2^- [M - H]^-$, calculated: 446.1622, found: 446.1596. Anal. Calcd. for $C_{27}H_{21}N_5O_2$: C, 72.47; H, 4.73; N, 15.65; found: C, 72.38; H, 4.88; N, 15.72%.

6-Amino-5-(4-chlorophenyl)-7-(4-methoxyphenyl)-2-phenyl-1,2,4-triazolo[1,5-a]pyridine-8-carbonitrile (15o) Pale yellow solid, mp 230–233 °C, yield: 89%. IR (KBr) ($\nu_{\max}/\text{cm}^{-1}$): 3330 and 3254 (NH_2), 2227 ($\text{C}\equiv\text{N}$), 1600, 1514, 1409, 1382, 1323, 1264, 1188, 1134, 1052, 1003, 979, 941, 832, 780, 625. ^1H NMR (500.1 MHz, $\text{DMSO}-d_6$): δ 8.18 (d, $J=8.4$ Hz, 2 H, 2CH), 8.04 (d, $J=8.1$ Hz, 2 H, 2CH), 7.95 (d, $J=8.5$ Hz, 2 H, 2CH), 7.79 (d, $J=8.5$ Hz, 2 H, 2CH), 7.60 (t, $J=7.9$ Hz, 2 H, 2CH), 7.42 (t, $J=7.6$ Hz, 1H, CH), 7.15 (d, $J=8.1$ Hz, 2 H, 2CH), 4.03 (s, 2 H, NH_2), 3.79 (s, 3 H, OCH_3). ^{13}C NMR (125.1 MHz, $\text{DMSO}-d_6$): δ 161.49, 153.29, 145.86, 140.39,

138.21, 136.28, 135.68, 133.63, 132.32, 129.88, 129.54, 126.46, 126.42, 124.27, 123.23, 117.53, 115.02, 113.04, 96.12, 56.26. HRMS (ESI) m/z for $C_{26}H_{17}ClN_5O^- [M - H]^-$, calculated: 450.1127, found: 450.1159. Anal. Calcd. for $C_{26}H_{18}ClN_5O$: C, 69.10; H, 4.01; N, 15.50; found: C, 69.22; H, 3.85; N, 15.59%.

6-Amino-7-(4-methoxyphenyl)-2-phenyl-5-(thiophen-2-yl)-1,2,4-triazolo[1,5-a]pyridine-8-carbonitrile (15p) Pale-yellow solid, mp 179–182 °C, yield: 66%. IR (KBr) ($\nu_{\max}/\text{cm}^{-1}$): 3335 and 3273 (NH_2), 2231 ($\text{C}\equiv\text{N}$), 1594, 1477, 1450, 1352, 1325, 1252, 1192, 1141, 1054, 959, 755, 702, 679. ^1H NMR (300.1 MHz, $\text{DMSO}-d_6$): δ 8.25 (dd, $J=4.9, 1.1$ Hz, 1H, CH), 8.16 (d, $J=8.2$ Hz, 2 H, 2CH), 8.04 (d, $J=8.4$ Hz, 2 H, 2CH), 7.99 (dd, $J=3.8, 1.1$ Hz, 1H, CH), 7.59 (t, $J=8.0$ Hz, 2 H, 2CH), 7.43 (dd, $J=4.9, 3.7$ Hz, 1H, CH), 7.39 (t, $J=7.6$ Hz, 1H, CH), 7.14 (d, $J=8.4$ Hz, 2 H, 2CH), 4.24 (s, 2 H, NH_2), 3.80 (s, 3 H, OCH_3). ^{13}C NMR (75.1 MHz, $\text{DMSO}-d_6$): δ 160.97, 153.51, 145.97, 141.41, 140.58, 136.21, 135.89, 134.40, 133.16, 130.04, 129.23, 126.75, 126.22, 123.51, 122.93, 114.62, 114.20, 112.84, 95.63, 55.88. HRMS (ESI) m/z for $C_{24}H_{16}N_5OS^- [M - H]^-$, calculated: 422.1081, found: 422.1104. Anal. Calcd. for $C_{24}H_{17}N_5OS$: C, 68.07; H, 4.05; N, 16.54; found: C, 68.16; H, 3.90; N, 16.69%.

6-Amino-7-(4-chlorophenyl)-2,5-diphenyl-1,2,4-triazolo[1,5-a]pyridine-8-carbonitrile (15q) Pale-yellow solid, mp 208–211 °C, yield: 78%. IR (KBr) ($\nu_{\max}/\text{cm}^{-1}$): 3350 and 3268 (NH_2), 2269 ($\text{C}\equiv\text{N}$), 1599, 1550, 1494, 1444, 1388, 1302, 1250, 1199, 1112, 1075, 1050, 827, 750, 642. ^1H NMR (500.1 MHz, $\text{DMSO}-d_6$): δ 8.25 (d, $J=8.0$ Hz, 2 H, 2CH), 8.11 (d, $J=8.6$ Hz, 2 H, 2CH), 8.04 (d, $J=7.7$ Hz, 2 H, 2CH), 7.91 (t, $J=7.2$ Hz, 1H, CH), 7.79 (t, $J=7.5$ Hz, 2 H, 2CH), 7.70 (d, $J=8.6$ Hz, 2 H, 2CH), 7.66 (t, $J=7.8$ Hz, 2 H, 2CH), 7.48 (t, $J=7.1$ Hz, 1H, CH), 4.38 (s, 2 H, NH_2). ^{13}C NMR (125.1 MHz, $\text{DMSO}-d_6$): δ 153.75, 145.40, 140.54, 137.09, 135.67, 135.14, 134.91, 133.97, 133.23, 130.81, 130.01, 129.65, 129.62, 126.59, 124.89, 123.37, 117.41, 114.21, 97.30. HRMS (ESI) m/z for $C_{25}H_{15}ClN_5^- [M - H]^-$, calculated: 420.1021, found: 420.1006. Anal. Calcd. for $C_{25}H_{16}ClN_5$: C, 71.17; H, 3.82; N, 16.60; found: C, 70.92; H, 4.04; N, 16.43%.

6-Amino-7-(4-chlorophenyl)-5-(4-methoxyphenyl)-2-phenyl-1,2,4-triazolo[1,5-a]pyridine-8-carbonitrile (15r) Pale-yellow solid, mp 223–226 °C, yield: 89%. IR (KBr) ($\nu_{\max}/\text{cm}^{-1}$): 3379 and 3233 (NH_2), 2254 ($\text{C}\equiv\text{N}$), 1599, 1548, 1504, 1450, 1418, 1325, 1241, 1202, 1141, 1116, 1031, 831, 800, 743. ^1H NMR (300.1 MHz, $\text{DMSO}-d_6$): δ 8.21 (d, $J=8.0$ Hz, 2 H, 2CH), 8.02 (d, $J=8.8$ Hz, 2 H, 2CH), 7.94 (d, $J=7.6$ Hz, 2 H, 2CH), 7.72–7.56 (m, 4 H, 4CH), 7.39 (t, $J=7.4$ Hz, 1H, CH), 7.24 (d, $J=7.6$ Hz, 2 H, 2CH), 4.32 (s, 2 H, NH_2), 3.88 (s, 3 H, OCH_3). ^{13}C NMR (75.1 MHz, $\text{DMSO}-d_6$): δ 159.96, 153.55, 145.15, 139.12, 136.88, 136.73, 133.61, 132.68, 130.04, 129.82, 129.41, 129.35, 126.36, 124.58, 123.59, 118.36, 114.54, 114.03, 97.12, 55.34. HRMS (ESI) m/z for $C_{26}H_{17}ClN_5O^- [M - H]^-$, calculated: 450.1127, found: 450.1099. Anal. Calcd. for $C_{26}H_{18}ClN_5O$: C, 69.10; H, 4.01; N, 15.50; found: C, 69.29; H, 4.12; N, 15.37%.

6-Amino-5,7-bis(4-chlorophenyl)-2-phenyl-1,2,4-triazolo[1,5-a]pyridine-8-carbonitrile (15s) Pale-yellow solid, mp 236–239 °C, yield: 84%. IR (KBr) ($\nu_{\max}/\text{cm}^{-1}$): 3329 and 3246 (NH_2), 2254 ($\text{C}\equiv\text{N}$), 1599, 1549, 1479, 1430, 1332, 1299, 1250, 1209, 1151, 1050, 804, 756, 732, 682. ^1H NMR (500.1 MHz, $\text{DMSO}-d_6$): δ 8.29 (d, $J=8.2$ Hz, 2 H, 2CH), 8.17 (d, $J=8.6$ Hz, 2 H, 2CH), 8.09 (d, $J=8.5$ Hz, 2 H, 2CH), 7.90 (d, $J=8.5$ Hz, 2 H, 2CH), 7.74 (d, $J=8.6$ Hz, 2 H, 2CH), 7.70 (t, $J=7.7$ Hz, 2 H, 2CH), 7.52 (t, $J=7.5$ Hz, 1H, CH), 4.47 (s, 2 H, NH_2). ^{13}C NMR (125.1 MHz, $\text{DMSO}-d_6$): δ 154.03, 145.66, 140.82, 139.07, 136.29, 136.04, 135.49, 135.12, 133.58, 133.01, 130.29, 130.00, 129.93, 126.87, 125.15, 123.65, 117.23, 114.49, 97.58. HRMS (ESI) m/z for $C_{25}H_{15}Cl_2N_5^- [M - H]^-$, calculated: 454.0632, found: 454.0643. Anal. Calcd. for $C_{25}H_{15}Cl_2N_5$: C, 65.80; H, 3.31; N, 15.35; found: C, 65.93; H, 3.14; N, 15.59%.

6-Amino-7-(4-chlorophenyl)-2-phenyl-5-(thiophen-2-yl)-1,2,4-triazolo[1,5-a]pyridine-8-carbonitrile (15t) Pale-yellow solid, mp 202–204 °C, yield: 77%. IR (KBr) ($\nu_{\max}/\text{cm}^{-1}$): 3351 and 3250 (NH_2), 2244 ($\text{C}\equiv\text{N}$), 1533, 1498, 1422, 1389, 1303, 1248, 1208, 1141, 1109, 1074, 1024, 865, 830, 748, 700, 647. ^1H NMR (500.1 MHz, $\text{DMSO}-d_6$): δ 8.38 (dd, $J=4.9, 0.9$ Hz, 1H, CH), 8.26 (d, $J=7.7$ Hz, 2 H, 2CH), 8.20–8.10 (m, 3 H, 3CH), 7.95 (d, $J=8.6$ Hz, 2 H, 2CH), 7.65 (d, $J=7.6$ Hz, 2 H, 2CH), 7.53 (t, $J=4.4$ Hz, 1H, CH), 7.47 (t, $J=7.2$ Hz, 1H, CH), 4.26 (s, 2 H, NH_2). ^{13}C NMR (125.1 MHz, $\text{DMSO}-d_6$): δ 153.61, 146.07, 141.68, 140.62, 137.52, 137.25, 136.06, 135.06, 134.60, 133.34, 130.10, 129.72, 126.69, 126.33, 123.46, 122.60, 114.89, 112.49, 95.79. HRMS (ESI) m/z for $C_{23}H_{13}ClN_5S^- [M - H]^-$, calculated: 426.0586, found: 426.0610. Anal. Calcd. for $C_{23}H_{14}ClN_5S$: C, 64.56; H, 3.30; N, 16.37; found: C, 65.69; H, 3.38; N, 16.54%.

6-Amino-2-(4-methoxyphenyl)-5,7-diphenyl-1,2,4-triazolo[1,5-a]pyridine-8-carbonitrile (15u) Pale-yellow solid, mp 196–199 °C, yield: 58%. IR (KBr) ($\nu_{\max}/\text{cm}^{-1}$): 3310 and 3214 (NH_2), 2232 ($\text{C}\equiv\text{N}$), 1582, 1531, 1498, 1449, 1381, 1298, 1239, 1201, 1142, 1115, 1073, 807, 740, 700, 633. ^1H NMR (500.1 MHz, $\text{DMSO}-d_6$): δ 8.11 (d, $J=8.2$ Hz, 2 H, 2CH), 8.01 (d, $J=8.4$ Hz, 2 H, 2CH), 7.94 (d, $J=7.6$ Hz, 2 H, 2CH), 7.73 (t, $J=7.8$ Hz, 1H, CH), 7.67 (t, $J=7.5$ Hz, 2 H, 2CH), 7.50–7.30 (m, 3 H, 3CH), 7.17 (d, $J=8.2$ Hz, 2 H, 2CH), 4.35 (s, 2 H, NH_2), 3.88 (s, 3 H, OCH_3). ^{13}C NMR (125.1 MHz, $\text{DMSO}-d_6$): δ 160.09, 152.97, 145.23, 136.77, 135.88, 135.01, 134.11, 133.49, 132.11, 132.01, 131.74, 131.13, 129.92, 129.72, 124.48, 118.78, 114.43, 114.10, 97.26, 55.10. HRMS (ESI) m/z for $C_{26}H_{18}N_5O^- [M - H]^-$, calculated: 416.1517, found: 416.1558. Anal. Calcd. for $C_{26}H_{19}N_5O$: C, 74.80; H, 4.59; N, 16.78; found: C, 74.72; H, 4.68; N, 16.76%.

6-Amino-2-(4-chlorophenyl)-5,7-diphenyl-1,2,4-triazolo[1,5-a]pyridine-8-carbonitrile (15v) Pale-yellow solid, mp 242–245 °C, yield: 71%. IR (KBr) ($\nu_{\max}/\text{cm}^{-1}$): 3382 and 3251 (NH_2), 2255 ($\text{C}\equiv\text{N}$), 1575, 1535, 1449, 1411, 1300, 1250, 1200, 1051, 1027, 813, 750, 722, 650. ^1H NMR (500.1 MHz, $\text{DMSO}-d_6$): δ 8.20 (d, $J=8.2$ Hz, 2 H, 2CH), 7.99 (d, $J=8.3$ Hz, 2 H, 2CH), 7.90 (d, $J=7.6$ Hz, 2 H, 2CH), 7.69 (t, $J=7.4$ Hz, 2 H, 2CH), 7.65 (t, $J=7.9$ Hz, 2 H, 2CH), 7.47–7.39 (m, 3 H, 3CH), 7.37 (d, $J=8.2$ Hz, 2 H, 2CH), 4.13 (s, 2 H, NH_2). ^{13}C NMR

(125.1 MHz, DMSO- d_6): δ 153.62, 145.86, 136.83, 136.32, 135.81, 134.56, 134.02, 132.85, 132.44, 131.68, 130.83, 130.39, 130.24, 129.80, 129.43, 124.82, 118.41, 114.59, 97.75. HRMS (ESI) m/z for $C_{25}H_{15}ClN_5^-$ [M - H] $^-$, calculated: 420.1021, found: 420.0986. Anal. Calcd. for $C_{25}H_{16}ClN_5$: C, 71.17; H, 3.82; N, 16.60; found: C, 71.32; H, 4.00; N, 16.72%.

α -Glucosidase inhibition assay

α -Glucosidase enzyme (EC3.2.1.20, *Saccharomyces cerevisiae*, 20 U/mg) and substrate (p-nitrophenyl glucopyranoside) were purchased from Sigma-Aldrich. Enzyme was prepared in potassium phosphate buffer (pH 6.8, 50 mM), as well as poly-substituted triazolopyridines **15a–15v** were dissolved in DMSO (10% final concentration). The various concentrations of these compounds (20 μ L), enzyme solution (20 μ L) and potassium phosphate buffer (135 μ L) were added in the 96-well plate and incubated at 37 °C for 10 min. Afterwards, the substrate (25 μ L, 4 mM) was added to the mentioned mixture and allowed to incubate at 37 °C for 20 min. Finally, the change in absorbance was measured at 405 nm by using spectrophotometer (Gen5, Power wave xs2, BioTek, America). The percentage of enzyme inhibition was calculated using Eq. (1) and IC_{50} values were obtained from non-linear regression curve using the Logit method.

$$\% \text{ Inhibition} = \frac{[Abs_{\text{control}} - Abs_{\text{sample}}] / Abs_{\text{control}}}{1} \times 100 \quad (1)$$

α -Amylase inhibition assay

To investigate the α -amylase inhibitory potency, 40 μ L of the triazolopyridine **15j** (dissolved in DMSO, with a final concentration of 100 μ M) and 40 μ L of α -amylase solution (0.5 mg/ml in sodium phosphate buffer, 0.006 M, pH 6.9, containing 0.02 M sodium chloride) were added to appropriate tubes and incubated at 25 °C for 10 min. Subsequently, 40 μ L of a starch solution (1% in 0.02 M sodium phosphate buffer) was added to each tube at 5-s intervals, followed by an additional 10-minute incubation at 25 °C. The reactions were then terminated by adding 100 μ L of dinitrosalicylic acid (DNS) reagent, and the tubes were placed in a boiling water bath for 5 min before cooling to room temperature. Under the same assessment, acarbose was tested. Afterward, the reaction mixtures were diluted with 900 μ L of distilled water, and absorbance was recorded at 540 nm.

Kinetic studies

The kinetic analysis was performed for the most potent compound (triazolopyridine **15j**) to reveal the inhibition mode against α -glucosidase. The 20 μ L of enzyme solution (1 U/mL) was incubated with different concentrations of compound **15j** (0, 1.6, 3.3, and 6.6 μ M) for 15 min at 30 °C. Afterwards, various concentrations of substrate (p-nitrophenyl glucopyranoside, 1 to 10 mM) was added to measure the change of absorbance for 20 min at 405 nm by using spectrophotometer (Gen5, Power wave xs2, BioTek, America).

In the presence of a competitive inhibitor, K_m increases while V_{max} does not change. Michaelis–Menten saturation curve for an enzyme reaction shows the relation between the substrate concentration and reaction rate as below:

$$\frac{v}{V_{\text{max}}} = \frac{[S]}{K_{m_{\text{app}}} + [S]} \quad (2)$$

According to Michaelis–Menten graph, $K_{m_{\text{app}}}$ is also defined as:

$$K_{m_{\text{app}}} = \left(1 + \frac{[I]}{K_I}\right) \quad (3)$$

[I] is the concentration of inhibitor.

Lineweaver Burk plot that provides a useful graphical method for analysis of the Michaelis–Menten is represented as:

$$\frac{1}{V_m} = \frac{K_m}{V_{\text{max}}} \left(1 + \frac{[I]}{K_I}\right) \frac{1}{[S]} + \frac{1}{V_{\text{max}}} \quad (4)$$

Therefore, the slope of Lineweaver Burk plot is equal to:

$$\text{Slope} = \frac{K_m}{V_{\text{max}}} \left(1 + \frac{[I]}{K_I}\right) \quad (5)$$

The $K_{m_{\text{app}}}$ value is calculated by Eq. (6):

$$K_{m_{\text{app}}} = K_m \left(1 + \frac{[I]}{K_I}\right) \quad (6)$$

Therefore, from replot of $K_{m_{\text{app}}}$ Vs. [I], Eq. (7) can be used for the calculation of K_I ^{60,61}:

$$K_{m_{\text{app}}} = K_m + \frac{K_m}{K_I} [I] \quad (7)$$

Computational studies

Data collection

In the current study, an extensive library of 1477 α -glucosidase inhibitors were extracted from the published articles. The compounds were derived from 100 parent molecules, each modified with various substituents to study structure-activity relationships. The synthesis and biological evaluation of the compounds occurred in a specialized laboratory setting with acarbose, as the positive control at almost 750 μ M concentration.

In order to identify the interactions of these compounds with the α -glucosidase, docking studies were carried out for all of them using the protein with PDB ID of 3A4A. All the docking simulations were carried out using the XP Glide module of the Schrödinger 14 suite. The methodology facilitated the detailed generation of molecular interaction fingerprints, offering valuable insights into the binding affinities and potential inhibitory mechanisms of the compounds. The vector consisted of fingerprint bits that indicated the presence or absence of interactions with each of the 589 residues across nine interaction types: 'contact,' 'backbone,' 'sidechain,' 'polar,' 'hydrophobic,' 'acceptor,' 'donor,' 'aromatic,' and 'charged,' yielding a final vector composed of 5301 bits.

During the docking process, multiple conformers were generated for certain compounds in various docked poses. To identify the most favorable conformer, several properties, including 'docking_score,' 'glide_ecoul,' 'glide_ligand_efficiency,' 'glide_emodel,' 'glide_evdw,' 'glide_XP_GScore,' and 'glide_XP_HBond,' were evaluated. For each property analyzed, the optimal conformer was selected, resulting in seven distinct sets, each representing the best conformers based on a specific property. These sets were subsequently analyzed and modeled to identify the overall most favorable set of conformers.

Additionally, 16 different types of structural fingerprints were calculated using the PyBiomed library to enhance and compare the performance of prediction models⁶². The study focused on binary classification models to predict the inhibitory activity of compounds. Based on IC_{50} values, the activity was categorized into two groups: inhibitors and weak inhibitors, with a threshold of 100 μ M used to differentiate between the two classes.

Data preprocess

To normalize the docking output, the MinMaxScaler library was applied to scale both positive and negative values to a range between -1 and 1 . This normalization ensured that all features contributed equally to the model training process, thereby improving the performance of the regression models. To improve the interaction fingerprints, the Variance Threshold library was employed to remove residues that exhibited no interactions across the dataset. This step removed features with no variance, reducing the dimensionality of the data and retaining only the most informative 269 bits for further analysis. Given the high dimensionality of the fingerprint vector, the MultiSURFStar feature selection algorithm was utilized to identify and retain the most relevant features, enhancing model performance and minimizing the risk of overfitting⁶³.

Modeling method

In this study, classification models were designed to predict the inhibitory activity of α -glucosidase inhibitors. The compounds were categorized as inhibitors or weak inhibitors based on an IC_{50} threshold of 100 μ M. Tree-based classification models were employed, and their performance was evaluated across seven collections of conformers to identify the most effective model and the fingerprint vectors with the highest predictive power.

To ensure reliable model performance, the dataset was divided into internal and external sets to prevent accidental data leakage into the test set. The external set consisted of 150 unique parent molecules and their substituents. A ten-fold cross-validation approach was employed for hyperparameter optimization, with model performance evaluated using the coefficient of determination (R^2), as defined in Eq. (8).

$$R^2 = 1 - \frac{\sum_{i=1}^n (y_i - \hat{y}')^2}{\sum_{i=1}^n (y_i - \bar{y}')^2} \quad (8)$$

Molecular docking protocol

The interactions of potential drug candidates with the protein were modeled through in silico molecular docking studies using the Glide tool within Schrödinger Suite 14.0. The protein structure, retrieved from the Protein Data Bank (PDB ID: 3A4A), was prepared using the Protein Preparation Wizard. This process included the addition of hydrogens, assignment of bond orders, and optimization of hydrogen bonding to ensure a realistic and accurate protein conformation. Ligands were prepared using the LigPrep module, which generated ionization states at physiological pH (7.0 ± 2.0). A grid box, centered on the co-crystallized ligand, was defined with dimensions of $20 \text{ \AA} \times 20 \text{ \AA} \times 20 \text{ \AA}$. Docking poses were ranked based on their GlideScore, which reflects the binding affinity of each ligand. Post-docking minimizations were carried out to refine the docking poses, followed by detailed interaction analyses using the XP Visualizer.

Molecular dynamic simulation

Molecular dynamics (MD) simulations were conducted using Desmond v2021.1 from the Schrödinger 2021-1 suite, accelerated by an NVIDIA RTX 3060 GPU, with preparation and analysis performed in Maestro for academic purposes. The protein-ligand complex was solvated using TIP3P water molecules within an orthorhombic box under periodic boundary conditions. A buffer distance of 10 \AA was added around the protein to ensure proper solvation. The system was neutralized by adding counter-ions and 0.15 M NaCl to mimic physiological conditions.

The MD protocol was divided into three stages: minimization, equilibration, and production. Minimization involved 2500 steps using the steepest descent algorithm, with convergence achieved when the maximum force

dropped below 1.0 kcal/mol/Å, ensuring optimum relaxation. Gradual equilibration was performed by heating the system from 0 K to 300 K using a small force constant to avoid structural collapse of the protein-ligand complex. The production phase, run under the NPT ensemble, maintained constant temperature (300 K) and pressure (1.01325 bar). Simulations were carried out for 200 ns, with frames saved every 1 ps to analyze dynamic behavior and structural changes over time.

Data availability

The authors confirm that the data supporting the finding of this study are available within the manuscript and supplementary file.

Received: 28 January 2025; Accepted: 8 May 2025

Published online: 22 May 2025

References

- Mekheimer, R. A., Sayed, A. A. R. & Ahmed, E. A. Novel 1, 2, 4-triazolo [1, 5-a] pyridines and their fused ring systems attenuate oxidative stress and prolong lifespan of caenorhabditis elegans. *J. Med. Chem.* **55**, 4169–4177. <https://doi.org/10.1021/jm2014315> (2012).
- Mekheimer, R. A., Sayed, A. A. R., Ahmed, E. A. & Sadek, K. U. Synthesis and characterization of new 1, 2, 4-Triazolo [1, 5-a] pyridines that extend the life span of caenorhabditis elegans via their Anti-Inflammatory/Antioxidant effects. *Arch. Pharm.* **348**, 650–665. <https://doi.org/10.1002/ardp.201500069> (2015).
- Mulwad, V. & Pawar, R. B. Synthesis of biologically active 5-benzopyranypyridines and triazolopyridines. (2003). <http://nopr.niscpr.res.in/handle/123456789/21765>
- Abudusaimi, M., Sun, F., Miyamoto, H. & Cheng, J. F. WO Patent 2013/029548, Jouve, Paris, FR. (2013).
- Kuroyanagi, J. et al. Novel antifungal agents: Triazolopyridines as inhibitors of β -1, 6-glucan synthesis. *Bioorg. Med. Chem.* **18**, 5845–5854. <https://doi.org/10.1016/j.bmc.2010.06.096> (2010).
- Kawakaki, K., Kanai, K., Fujisawa, T., Morita, C. & Suzuki, T. EP Patent 1717238A1, Jouve, Paris, FR. (2006).
- Shaik, K. et al. 7-Amino-2-aryl/hetero-aryl-5-oxo-5, 8-dihydro [1, 2, 4] Triazolo [1, 5-a] pyridine-6-carbonitriles: synthesis and adenosine receptor binding studies. *Chem. Biol. Drug Des.* **94**, 1568–1573. <https://doi.org/10.1111/cbdd.13528> (2019).
- Nakajima, R. et al. Discovery of [1, 2, 4] Triazolo [1, 5-a] pyridine derivatives as potent and orally bioavailable ROR γ t inverse agonists. *ACS Med. Chem. Lett.* **11**, 528–534. <https://doi.org/10.1021/acsmchemlett.9b00649> (2020).
- Flohr, K. et al. WO Patent 2013/178572, WIPO, Switzerland (2013).
- Wu, L. et al. WO Patent. / 070089, WIPO, Switzerland 2017 (2017).
- Felts, A. S. et al. Discovery of Imidazo [1, 2-a]-, [1, 2, 4] Triazolo [4, 3-a]-, and [1, 2, 4] Triazolo [1, 5-a] pyridine-8-carboxamide negative allosteric modulators of metabotropic glutamate receptor subtype 5. *Bioorg. Med. Chem. Lett.* **27**, 4858–4866. <https://doi.org/10.1016/j.bmcl.2017.09.042> (2017).
- Song, W. et al. [1, 2, 4] Triazolo [1, 5-a] pyridine-based host materials for green phosphorescent and delayed-fluorescence OLEDs with low efficiency roll-off. *ACS Appl. Mater. Interfaces.* **10**, 24689–24698. <https://doi.org/10.1021/acsami.8b07462> (2018).
- Van de Laar, F. A. et al. Alpha-glucosidase inhibitors for type 2 diabetes mellitus. *Cochrane Database Syst. Rev.* <https://doi.org/10.1002/14651858.CD003639.pub2> (2005).
- Bouchi, R. et al. A consensus statement from the Japan diabetes society (JDS): a proposed algorithm for pharmacotherapy in people with type 2 diabetes—2nd edition (English version). *Diabetol. Int.* **15**, 327–345. <https://doi.org/10.1007/s13340-024-00723-8> (2024).
- DiNicolantonio, J. J., Bhutani, J. & O’Keefe, J. H. Acarbose: safe and effective for lowering postprandial hyperglycaemia and improving cardiovascular outcomes. *Open. Heart.* **2**, e000327. <https://doi.org/10.1136/openhrt-2015-000327> (2015).
- Adib, M. et al. Design and synthesis of new fused carbazole-imidazole derivatives as anti-diabetic agents: in vitro α -glucosidase inhibition, kinetic, and in Silico studies. *Bioorg. Med. Chem. Lett.* **29**, 713–718. <https://doi.org/10.1016/j.bmcl.2019.01.012> (2019).
- Peytam, F. et al. Design and synthesis of new Imidazo [1, 2-b] pyrazole derivatives, in vitro α -glucosidase Inhibition, kinetic and Docking studies. *Mol. Divers.* **24**, 69–80. <https://doi.org/10.1007/s11030-019-09925-8> (2020).
- Peytam, F. et al. Synthesis and biological evaluation of new Dihydroindolizino [8, 7-b] Indole derivatives as novel α -glucosidase inhibitors. *J. Mol. Struct.* **1224**, 129290. <https://doi.org/10.1016/j.molstruc.2020.129290> (2021).
- Singh, A. et al. Recent developments in synthetic α -glucosidase inhibitors: A comprehensive review with structural and molecular insight. *J. Mol. Struct.* **1281**, 135115. <https://doi.org/10.1016/j.molstruc.2023.135115> (2023).
- Mushtaq, A., Azam, U., Mehreen, S. & Naseer, M. M. Synthetic α -glucosidase inhibitors as promising anti-diabetic agents: recent developments and future challenges. *Eur. J. Med. Chem.* **249**, 115119. <https://doi.org/10.1016/j.ejmech.2023.115119> (2023).
- Pan, G. et al. A review on the in vitro and in vivo screening of α -glucosidase inhibitors. *Heliyon* <https://doi.org/10.1016/j.heliyon.2024.e37467> (2024).
- Moghimi, S. et al. Design and synthesis of novel pyridazine N-aryl acetamides: In-vitro evaluation of α -glucosidase Inhibition, docking, and kinetic studies. *Bioorg. Chem.* **102**, 104071. <https://doi.org/10.1016/j.bioorg.2020.104071> (2020).
- Peytam, F. et al. An efficient and targeted synthetic approach towards new highly substituted 6-amino-pyrazolo [1, 5-a] pyrimidines with α -glucosidase inhibitory activity. *Sci. Rep.* **10**, 2595. <https://doi.org/10.1038/s41598-020-59079-z> (2020).
- Peytam, F. et al. Design, synthesis, molecular docking, and in vitro α -glucosidase inhibitory activities of novel 3-amino-2, 4-diarylbenzo [4, 5] Imidazo [1, 2-a] pyrimidines against yeast and rat α -glucosidase. *Sci. Rep.* **11**, 11911. <https://doi.org/10.1038/s41598-021-91473-z> (2021).
- Peytam, F. et al. Imidazo [1, 2-c] Quinazolines as a novel and potent scaffold of α -glucosidase inhibitors: design, synthesis, biological evaluations, and in Silico studies. *Sci. Rep.* **13**, 15672. <https://doi.org/10.1038/s41598-023-42549-5> (2023).
- Firoozpour, L. et al. Synthesis, α -Glucosidase inhibitory activity and Docking studies of novel Ethyl 1, 2, 3-triazol-4-ylmethylthio-5, 6-diphenylpyridazine-4-carboxylate derivatives. *BMC Chem.* **17**, 66. <https://doi.org/10.1186/s13065-023-00973-8> (2023).
- Peytam, F. et al. Design, synthesis, and evaluation of novel substituted Imidazo [1, 2-c] Quinazoline derivatives as potential α -glucosidase inhibitors with bioactivity and molecular Docking insights. *Sci. Rep.* **14**, 27507. <https://doi.org/10.1038/s41598-024-78878-2> (2024).
- Carlucci, R., Lisa, M. N. & Labadie, G. R. 1, 2, 3-Triazoles in biomolecular crystallography: A geometrical Data-Mining approach. *J. Med. Chem.* **66**, 14377–14390. <https://doi.org/10.1021/acs.jmedchem.3c01097> (2023).
- Khan, J. et al. Exploring triazole-based drugs: synthesis, application, FDA approvals, and clinical trial updates-A comprehensive review. *Tetrahedron.* 134122 (2024).
- Gupta, O., Pradhan, T. & Chawla, G. An updated review on diverse range of biological activities of 1, 2, 4-triazole derivatives: insight into structure activity relationship. *J. Mol. Struct.* **1274**, 134487 (2023).
- Ajmal, M. et al. Significance of Triazole in medicinal chemistry: advancement in drug design, reward and biological activity. *Chem. Biodivers.* **21**, e202400637. <https://doi.org/10.1002/cbdv.202400637> (2024).

32. Karypidou, K. et al. Synthesis, biological evaluation and molecular modeling of a novel series of fused 1, 2, 3-triazoles as potential anti-coronavirus agents. *Bioorg. Med. Chem. Lett.* **28**, 3472–3476. <https://doi.org/10.1016/j.bmcl.2018.09.019> (2018).
33. Matin, M. M. et al. Triazoles and their derivatives: chemistry, synthesis, and therapeutic applications. *Front. Mol. Biosci.* **9**, 864286. <https://doi.org/10.3389/fmolb.2022.864286> (2022).
34. Chirra, S. et al. Synthesis of [1, 2, 4] Triazolo [3, 4-b][1, 3, 4] thiadiazine-1, 2, 3-triazoles as potent EGFR targeting anti-breast cancer agents. *J. Mol. Struct.* **1306**, 137803. <https://doi.org/10.1016/j.molstruc.2024.137803> (2024).
35. Bandi, S. R. et al. Synthesis and biological evaluation of novel [1, 2, 3] triazolo-pyrrolo [1, 2-a] pyrido [4, 3-d] pyrimidines as EGFR targeting anticancer agents. *J. Mol. Struct.* **1274**, 134378. <https://doi.org/10.1016/j.molstruc.2022.134378> (2023).
36. Sucharitha, E. R., Krishna, T. M., Manchal, R., Ramesh, G. & Narsimha, S. Fused benzo [1, 3] thiazine-1, 2, 3-triazole hybrids: Microwave-assisted one-pot synthesis, in vitro antibacterial, antibiofilm, and in Silico ADME studies. *Bioorg. Med. Chem. Lett.* **47**, 128201. <https://doi.org/10.1016/j.bmcl.2021.128201> (2021).
37. Kumar, M., Nukala, S. K., Krishna, T. M. & Narsimha, S. Benzothiazole-[1, 2, 3] Triazolo [5, 1-a] isoindoles: synthesis, anticancer activity, bioavailability and in Silico studies against Gama-Tubulin protein. *J. Mol. Struct.* **1250**, 131722. <https://doi.org/10.1016/j.molstruc.2021.131722> (2022).
38. Sharma, A. et al. An insight on medicinal attributes of 1, 2, 3-and 1, 2, 4-triazole derivatives as alpha-amylase and alpha-glucosidase inhibitors. *Mol. Divers.* 1–30. <https://doi.org/10.1007/s11030-023-10728-1> (2023).
39. Khomenko, D. M. et al. An alternative approach to the synthesis of [1, 2, 4] Triazolo [1, 5-a] pyridine-8-carbonitriles, their crystal structure, and DFT calculations. *J. Heterocycl. Chem.* **58**, 1278–1285. <https://doi.org/10.1002/jhet.4256> (2021).
40. Volovenko, Y. M. & Shokol, T. Convenient method for the annelation of a pyridine ring to azaheterocyclic systems. *Chem. Heterocycl. Compd.* **39** <https://doi.org/10.1023/A:1024738018872> (2003).
41. Trottmann, G. H. et al. inventor; Hoffmann-La Roche Inc., assignee. Amino-triazolopyridine Derivatives. US 6355653, March 12 (2002).
42. Milokhov, D. S. et al. Hydroxypropyl substituted nitrogen bridgehead fused cyanopyridines. *Tetrahedron* **70**, 1214–1222. <https://doi.org/10.1016/j.tet.2013.12.074> (2014).
43. Zribi, L., Zribi, F., Marco-Contelles, J., Chabchoub, F. & Ismaili, L. Facile one-pot synthesis of new [1, 2, 4] Triazolo [1, 5-a] pyridine derivatives by ultrasonic irradiation. *Synth. Commun.* **47**, 1934–1939. <https://doi.org/10.1080/00397911.2017.1357078> (2017).
44. Shao, J. et al. Tuning the annulation reactivity of vinyl Azides and carbazates: A divergent synthesis of aza-pyrimidinones and imidazoles. *Org. Lett.* **17**, 4502–4505. <https://doi.org/10.1021/acs.orglett.5b02180> (2015).
45. Shu, K. et al. Base-mediated synthesis of highly functionalized 2-aminonicotinonitriles from α -keto vinyl Azides and α -dicyanoalkenes. *RSC Adv.* **6**, 49123–49126. <https://doi.org/10.1039/C6RA04669J> (2016).
46. Adib, M., Peytam, F., Rahmanian-Jazi, M., Bijanzadeh, H. R. & Amanlou, M. A new synthetic strategy towards 2, 4, 5-trisubstituted 1H-imidazoles and highly substituted Pyrrolo [1, 2-c] imidazoles by use of α -azidochalcones via Michael addition-cyclization followed by Wittig reaction. *Tetrahedron* **73**, 6696–6705. <https://doi.org/10.1016/j.tet.2017.09.042> (2017).
47. Rajaguru, K., Mariappan, A., Muthusubramanian, S. & Bhuvanesh, N. Divergent reactivity of α -azidochalcones with metal β -diketonates: tunable synthesis of substituted pyrroles and Indoles. *Org. Chem. Front.* **4**, 124–129. <https://doi.org/10.1039/C6QO00541A> (2017).
48. Adib, M. et al. Design, synthesis and in vitro α -glucosidase Inhibition of novel coumarin-pyridines as potent antidiabetic agents. *New J. Chem.* **42**, 17268–17278. <https://doi.org/10.1039/C8NJ02495B> (2018).
49. Adib, M. et al. New 6-amino-pyrido [2, 3-d] pyrimidine-2, 4-diones as novel agents to treat type 2 diabetes: a simple and efficient synthesis, α -glucosidase Inhibition, molecular modeling and kinetic study. *Eur. J. Med. Chem.* **155**, 353–363. <https://doi.org/10.1016/j.ejmech.2018.05.046> (2018).
50. Borra, S., Chandrasekhar, D., Newar, U. D. & Maurya, R. A. Access to 2, 3-fused pyrroles via visible light driven coupling of α -azidochalcones with 1/2-naphthols, or 2-hydroxy-1, 4-naphthoquinone. *J. Org. Chem.* **84**, 1042–1052. <https://doi.org/10.1021/acs.joc.8b02459> (2018).
51. Adib, M. & Peytam, F. An efficient synthesis of fully substituted Pyrazolo [3, 4-b] pyridin-5-amines from α -azidochalcones. *Tetrahedron* **74**, 2414–2420. <https://doi.org/10.1016/j.tet.2018.03.036> (2018).
52. Peytam, F. et al. A one-pot and three-component synthetic approach for the Preparation of asymmetric and multi-substituted 1, 4-dihydropyrazines. *Tetrahedron Lett.* **60**, 151257. <https://doi.org/10.1016/j.tetlet.2019.151257> (2019).
53. Newar, U. D., Borra, S. & Maurya, R. A. Visible-light 2, 4-dinitrophenol-mediated photoannulation of α -azidochalcones into 2, 5-diaryloxazoles. *Org. Lett.* **24**, 4454–4458. <https://doi.org/10.1021/acs.orglett.2c01691> (2022).
54. Devi Newar, U., Boruah, J., Awatar Maurya, D. & R Recent advances in the use of α -Azidochalcones in heterocycle synthesis. *Adv. Synth. Catal.* **366**, 2859–2897. <https://doi.org/10.1002/adsc.202400150> (2024).
55. Li, K. et al. Inhibitory effects against α -glucosidase and α -amylase of the flavonoids-rich extract from *Scutellaria baicalensis* shoots and interpretation of structure–activity relationship of its eight flavonoids by a refined assign-score method. *Chem. Cent. J.* **12**, 1–11. <https://doi.org/10.1186/s13065-018-0445-y> (2018).
56. Kazempour-Dizaji, M. et al. Arylureidoaurones: synthesis, in vitro α -glucosidase, and α -amylase Inhibition activity. *Bioorg. Chem.* **139**, 106709. <https://doi.org/10.1016/j.bioorg.2023.106709> (2023).
57. Odugbemi, A. I., Nyirenda, C., Christoffels, A. & Egieyeh, S. A. Artificial intelligence in antidiabetic drug discovery: the advances in QSAR and the prediction of α -glucosidase inhibitors. *Comput. Struct. Biotechnol. J.* <https://doi.org/10.1016/j.csbj.2024.07.003> (2024).
58. Yadav, V. K. & Babu, K. G. A remarkably efficient Markovnikov hydrochlorination of olefins and transformation of nitriles into imidates by use of accl and an alcohol. *Eur. J. Org. Chem.* **2005**, 452–456. <https://doi.org/10.1002/ejoc.200400591> (2005).
59. Edraki, N. et al. 2-Imino 2 H-chromene and 2-(phenylimino) 2 H-chromene 3-aryl Carboxamide derivatives as novel cytotoxic agents: synthesis, biological assay, and molecular Docking study. *J. Iran. Chem. Soc.* **13**, 2163–2171. <https://doi.org/10.1007/s13738-016-0934-7> (2016).
60. Dixon, M. The determination of enzyme inhibitor constants. *Biochem. J.* **55**, 170. <https://doi.org/10.1042/bj0550170> (1953).
61. Todd, M. J. & Hausinger, R. Competitive inhibitors of *Klebsiella* aerogenes urease: mechanisms of interaction with the nickel active site. *J. Biol. Chem.* **264**, 15835–15842. [https://doi.org/10.1016/S0021-9258\(18\)71553-6](https://doi.org/10.1016/S0021-9258(18)71553-6) (1989).
62. Dong, J. et al. PyBioMed: a python library for various molecular representations of chemicals, proteins and DNAs and their interactions. *J. Cheminform.* **10**, 1–11. <https://doi.org/10.1186/s13321-018-0270-2> (2018).
63. Arabi, N., Torabi, M. R., Fassih, A. & Ghasemi, F. Identification of potential vascular endothelial growth factor receptor inhibitors via tree-based learning modeling and molecular Docking simulation. *J. Chemometrics: E.* **3545**. <https://doi.org/10.1002/cem.3545> (2024).

Acknowledgements

This work was supported by a grant from the research council of Tehran University of Medical Sciences, Tehran, Iran grant No. 1402-3-104-68654.

Author contributions

A.F., L.F., and F.P. designed the study and conducted the experiments. F.P. and P.F. synthesized the targeted compounds and wrote the manuscript. H.O.G. and M.N. analyzed the characterization data and prepared the Supporting Information File. S.M. and M.A.F. performed the in vitro enzymatic analysis and kinetic study. F.G. and M.T. carried out the computational studies. B.B. and M.B.T. revised the manuscript.

Declarations

Competing interests

The authors declare no competing interests.

Additional information

Supplementary Information The online version contains supplementary material available at <https://doi.org/10.1038/s41598-025-01819-0>.

Correspondence and requests for materials should be addressed to L.F. or A.F.

Reprints and permissions information is available at www.nature.com/reprints.

Publisher's note Springer Nature remains neutral with regard to jurisdictional claims in published maps and institutional affiliations.

Open Access This article is licensed under a Creative Commons Attribution-NonCommercial-NoDerivatives 4.0 International License, which permits any non-commercial use, sharing, distribution and reproduction in any medium or format, as long as you give appropriate credit to the original author(s) and the source, provide a link to the Creative Commons licence, and indicate if you modified the licensed material. You do not have permission under this licence to share adapted material derived from this article or parts of it. The images or other third party material in this article are included in the article's Creative Commons licence, unless indicated otherwise in a credit line to the material. If material is not included in the article's Creative Commons licence and your intended use is not permitted by statutory regulation or exceeds the permitted use, you will need to obtain permission directly from the copyright holder. To view a copy of this licence, visit <http://creativecommons.org/licenses/by-nc-nd/4.0/>.

© The Author(s) 2025